

Article

Fragment-based discovery of a potent, orally bioavailable inhibitor which modulates the phosphorylation and catalytic activity of ERK1/2

Tom D. Heightman, Valerio Berdini, Hannah Braithwaite, Ildiko Maria Buck, Megan Cassidy, Juan Castro, Aurelie Courtin, James E. H. Day, Charlotte East, Lynsey Fazal, Brent Graham, Charlotte M. Griffiths-Jones, John F Lyons, Vanessa Martins, Sandra Muench, Joanne M Munck, David Norton, Marc O'Reilly, Nick Palmer, Puja Pathuri, Michael Reader, David C. Rees, Sharna J. Rich, Caroline Richardson, Harpreet Saini, Neil T Thompson, Nicola G Wallis, Hugh Walton, Nicola E. Wilsher, Alison J.-A. Woolford, Michael Cooke, David Cousin, Stuart Onions, Jonathan Shannon, John Watts, and Christopher W Murray

J. Med. Chem., **Just Accepted Manuscript** • DOI: 10.1021/acs.jmedchem.8b00421 • Publication Date (Web): 18 May 2018

Downloaded from <http://pubs.acs.org> on May 18, 2018

Just Accepted

“Just Accepted” manuscripts have been peer-reviewed and accepted for publication. They are posted online prior to technical editing, formatting for publication and author proofing. The American Chemical Society provides “Just Accepted” as a service to the research community to expedite the dissemination of scientific material as soon as possible after acceptance. “Just Accepted” manuscripts appear in full in PDF format accompanied by an HTML abstract. “Just Accepted” manuscripts have been fully peer reviewed, but should not be considered the official version of record. They are citable by the Digital Object Identifier (DOI®). “Just Accepted” is an optional service offered to authors. Therefore, the “Just Accepted” Web site may not include all articles that will be published in the journal. After a manuscript is technically edited and formatted, it will be removed from the “Just Accepted” Web site and published as an ASAP article. Note that technical editing may introduce minor changes to the manuscript text and/or graphics which could affect content, and all legal disclaimers and ethical guidelines that apply to the journal pertain. ACS cannot be held responsible for errors or consequences arising from the use of information contained in these “Just Accepted” manuscripts.

1
2
3
4
5
6
7
8
9
10
11
12
13
14
15
16
17
18
19
20
21
22
23
24
25
26
27
28
29
30
31
32
33
34
35
36
37
38
39
40
41
42
43
44
45
46
47
48
49
50
51
52
53
54
55
56
57
58
59
60

	Cousin, David; Sygnature Discovery Ltd Onions, Stuart; Sygnature Discovery Ltd Shannon, Jonathan; Sygnature Discovery Ltd Watts, John; Sygnature Discovery Ltd Murray, Christopher; Astex Pharamceuticals,

SCHOLARONE™
Manuscripts

1
2
3 **Fragment-based discovery of a potent, orally bioavailable inhibitor which**
4
5 **modulates the phosphorylation and catalytic activity of ERK1/2**
6
7

8 Tom D. Heightman,^{1,*} Valerio Berdini,¹ Hannah Braithwaite,¹ Ildiko M. Buck,¹ Megan Cassidy,¹ Juan
9 Castro,¹ Aurélie Courtin,¹ James E.H. Day,¹ Charlotte East,¹ Lynsey Fazal,¹ Brent Graham,¹ Charlotte
10 M. Griffiths-Jones,¹ John F. Lyons,¹ Vanessa Martins,¹ Sandra Muench,¹ Joanne M. Munck,¹ David
11 Norton,¹ Marc O'Reilly,¹ Nick Palmer,¹ Puja Pathuri,¹ Michael Reader,¹ David C. Rees,¹ Sharna J.
12 Rich,¹ Caroline Richardson,¹ Harpreet Saini,¹ Neil T. Thompson,¹ Nicola G. Wallis,¹ Hugh Walton,¹
13 Nicola E. Wilsher,¹ Alison J.-A. Woolford,¹ Michael Cooke,² David Cousin,² Stuart Onions,²
14 Jonathan Shannon,² John Watts,² and Christopher W. Murray¹
15
16
17
18
19
20
21
22

23 ¹ Astex Pharmaceuticals, 436 Cambridge Science Park, Cambridge, CB4 0QA, UK
24

25 ² Sygnature Discovery Ltd, BioCity, Pennyfoot Street, Nottingham, NG1 1GF, UK
26

27 * Corresponding author
28
29
30
31
32
33
34
35
36
37
38
39
40
41
42
43
44
45
46
47
48
49
50
51
52
53
54
55
56
57
58
59
60

ABSTRACT

Aberrant activation of the MAPK pathway drives cell proliferation in multiple cancers. Inhibitors of BRAF and MEK kinases are approved for the treatment of BRAF mutant melanoma, but resistance frequently emerges, often mediated by increased signalling through ERK1/2. Here we describe the fragment based generation of ERK1/2 inhibitors which block catalytic phosphorylation of downstream substrates such as RSK but also modulate phosphorylation of ERK1/2 by MEK without directly inhibiting MEK. X-ray crystallographic and biophysical fragment screening followed by structure-guided optimization and growth from the hinge into a pocket proximal to the C- α helix afforded highly potent ERK1/2 inhibitors with excellent kinome selectivity. In BRAF mutant cells the lead compound suppresses pRSK and pERK levels and inhibits proliferation at low nanomolar concentrations. The lead exhibits tumor regression upon oral dosing in BRAF mutant xenograft models, providing a promising basis for further optimization towards clinical pERK1/2 modulating ERK1/2 inhibitors.

INTRODUCTION

The extracellular signal-related kinases 1 and 2 (ERK1/2) are highly homologous serine/threonine kinases that form a key node in the transduction of growth factor signals, regulating a range of cellular functions including cell survival, differentiation, adhesion, migration and proliferation.¹ Of particular relevance to oncology, the RAS-RAF-MEK-ERK signalling cascade (MAPK pathway) is activated through mutations in RAS or RAF in over 30% of cancers including melanoma, lung, pancreatic and colorectal (CRC) cancer.² Although RAS has proven refractory to drug targeting for many years, the successful development of inhibitors of BRAF and MEK1/2 kinases has led to effective treatment particularly of melanomas whose tumor growth is driven by activating mutations in BRAF such as V600E.³ Despite these successes, resistance often emerges after several months leading to increased signalling through ERK1/2.^{4,5}

Human ERK1 and ERK2 are 84% identical in sequence and show some redundancy in cellular function, although some studies have suggested that ERK2 plays the dominant role in driving cell proliferation.^{6,7,8-9} ERK1/2 are activated by MEK1/2 through sequential dual phosphorylation of Tyr187 and Thr185 residues in the ERK1/2 activation loop. Diphosphorylation of ERK1/2 triggers two distinct modes of function.¹⁰ Firstly, the activated ERK1/2 catalyse the phosphorylation of numerous cytosolic downstream substrates, including RSK which is commonly used as a biomarker for ERK1/2 activity and inhibition. Secondly, the phosphorylation of ERK1/2 leads to their translocation to the nucleus, where they phosphorylate and activate nuclear substrates including transcription factors.

Motivated by the importance of the ERK1/2 signaling cascade in cancer and the validation through approved inhibitors of BRAF and MEK, multiple groups have targeted ERK1/2 inhibitors, including several reaching clinical trials (Figure 1) (ulixertinib (**1**),¹¹ GDC-0994 (**2**),¹² MK-8353,¹³ LY3214996 (**3**),¹⁴ LTT462,¹⁵ KO-947,¹⁶ and others disclosed.^{17-20 21 22 23} Among the clinical studies completed to date, ulixertinib reported responses in BRAF V600 and non-V600 mutant solid tumors including melanoma, glioblastoma multiforme, lung cancers with brain metastases, gallbladder and head & neck

1
2
3 cancers;²⁴ while MK-8353 showed responses in BRAF V600-mutant melanoma.²⁵ The majority of
4
5 clinical ERK inhibitors are ATP competitive, blocking the catalytic activity of ERK1/2, but do not
6
7 prevent its phosphorylation by MEK, and hence do not prevent the nuclear localisation of pERK. The
8
9 series of compounds represented by SCH772984 (**4**, Figure 1) published by Schering/Merck, and
10
11 structurally related to MK-8353, showed the ability to inhibit both the catalytic activity of ERK1/2
12
13 and their phosphorylation by MEK.²⁶ This dual pharmacology might be expected to more completely
14
15 suppress MAPK pathway signalling, with potential benefits in terms of efficacy and emergence of
16
17 resistance.

18
19 We sought to assess the potential benefits of the dual inhibition-pERK modulation profile in *in vivo*
20
21 models, but were unable to achieve good exposure levels following oral or i.p. dosing of **4**, prompting
22
23 us to seek an alternative chemotype with similar pharmacology. Crystal structural studies performed
24
25 by us (*vide infra*) and others²⁷ on **4** suggested that it binds to an altered conformation of ERK2, in
26
27 which Tyr36 in the glycine-rich loop (P-loop) becomes tucked under the loop, allowing the extended
28
29 structure of the inhibitor to occupy a second pocket. We hypothesized that the binding mode of **4**
30
31 might underlie its ability to block the phosphorylation of ERK1/2, and initiated a fragment-based
32
33 approach to develop orally bioavailable ERK1/2 inhibitors which bind to a similar conformation of
34
35 ERK1/2 and which also modulate the phosphorylation of ERK1/2.

40 41 **RESULTS AND DISCUSSION**

42 *Fragment screen and structural insights*

43
44 Given the high sequence similarity between ERK1 and 2, we used ERK2 for structural and SAR
45
46 studies. In order to obtain crystals of human ERK2 for fragment and inhibitor structural analysis,
47
48 conditions similar to those published for expression, purification and crystallization¹⁸ were used.

49
50
51 By soaking crystals of ERK2 in a solution of **4**, a 2.3Å co-structure was obtained. The structure is
52
53 similar to that subsequently published.²⁷ Of particular note is the occupancy of a second pocket in
54
55 ERK2 upon binding SCH772984. In structures of ERK2 bound with ATP-competitive hinge binding
56
57

1
2
3 inhibitors such as ulixertinib, Tyr36 on the glycine-rich loop is involved in a pi-pi stacking interaction
4
5 with Tyr64 on the C- α helix (“out” conformation, Figure 2a). By contrast, in order to accommodate
6
7 the aromatic tail portion of **4**, the glycine-rich loop undergoes a conformational change in which
8
9 Tyr36 tucks under the loop and stacks on the hydrophobic side of the pyrrolidine ring of **4** (“in”
10
11 conformation, Figure 2b). The pyrimidine ring of the inhibitor mimics Tyr36 by engaging in a
12
13 stacking interaction with Tyr64. The central pyrrolidine nitrogen and two amide carbonyl oxygens of
14
15 **4** also mediate an unusual tridentate interaction with Lys54.

16
17 A recently published NMR study showed the presence of multiple conformational states for ERK2 in
18
19 solution, depending on the phosphorylation state.²⁸ This work provided evidence that the distribution
20
21 of conformational states could be altered in the presence of the Vertex inhibitor **11e** (Supplementary
22
23 Figure 1), closely related to ulixertinib, favouring the active conformation of ERK2 when the enzyme
24
25 is doubly phosphorylated. These findings supported the notion that changes in ERK1/2
26
27 conformational distributions in response to different inhibitor binding modes might influence
28
29 molecular recognition by ERK and by extension the phosphorylation state.

30
31 A crystallographic screen of our corporate fragment collection was conducted by soaking crystals of
32
33 ERK2 in solutions of fragments. In addition, a screen using thermal melt (differential scanning
34
35 fluorimetry, DSF) was carried out, together with a virtual library screen. Hits from these methods
36
37 were evaluated for inhibitory potency in an ERK2 bioassay. These approaches led to the identification
38
39 of several fragments binding to ERK2, including the pyrazolyl aminopyrimidine fragment **5**, which
40
41 binds to the hinge of ERK2 (Figure 2c); and aminoindazole fragment **6**, which binds not only to the
42
43 hinge but also in the second pocket between the P-loop and C- α helix (Figure 2d). Interestingly,
44
45 binding of fragment **6** elicits a third conformation of Tyr36 in which it is pushed away from Tyr64
46
47 towards solvent. The fact that Tyr36 could be displaced to allow such a small, weakly binding
48
49 fragment to occupy the second pocket suggests a significant conformational flexibility in the ERK2 P-
50
51 loop. This structure was also useful as it provided additional insights with which to design inhibitors
52
53 occupying this pocket.
54
55
56
57
58
59
60

1
2
3 Among the hinge binding fragment hits, fragment **5** showed promising affinity and ligand efficiency
4 (Table 1), with attractive synthetic vectors for further optimization and elaboration. The structure of
5 fragment **5** bound to ERK2 indicated several key interactions with the protein which drive its affinity
6 (Figure 3a). Hydrogen bonds were observed between the pyrimidine N and amino NH of the fragment
7 and the ERK2 backbone NH and C=O of hinge residue Met108 respectively. In addition, the pyrazole
8 nitrogen accepts a hydrogen bond from Lys114. The methyl group of the pyrimidine points towards
9 the side chain of the gatekeeper residue Gln105.
10
11

12
13
14
15
16
17 Prior to growing further into the ATP binding site, we considered two features to guide our initial
18 optimisation of fragment **5**. First, we explored replacing the pyrazole moiety with an oxan (THP), in
19 order to increase the sp³ content of the fragment and mitigate against potential future solubility
20 problems in more elaborated lead molecules. The resulting fragment **7** showed a >10-fold increase in
21 affinity and ligand efficiency (Table 1). Second, given the close proximity of the pyrimidine methyl
22 group to the side chain of gatekeeper residue Gln105, we explored the effects of larger and smaller
23 groups in this position. The data for fragments **8-10**, containing hydrogen, fluoro or chloro
24 respectively, indicated a preference for larger substituents (Table 1), such that the chloro-substituent
25 gave a modest increase in affinity, attributable to a halogen bonding interaction between the Cl sigma
26 hole and the Gln105 side chain carbonyl oxygen. The structure of chloropyrimidine oxanyl fragment
27 **10** shows similar interactions with the hinge residues as fragment **5**, but an altered conformation of the
28 side chain of Lys114 in order to achieve a hydrogen bond between the 4-oxanyl oxygen and the Lys ε-
29 amino group (Figure 3b, c).
30
31
32
33
34
35
36
37
38
39
40
41
42
43

44 *Growth towards the gatekeeper: identification of the isoindolinone core*

45
46
47 Having identified a potent and ligand efficient hinge binder in fragment **10**, we next sought to grow
48 across the ATP binding site towards the second pocket. Prototypical ERK inhibitors such as
49 ulixertinib avoid the introduction of an additional hydrogen bond donor into the inhibitor to interact
50 with the gatekeeper carbonyl oxygen by exploiting a water-bridged interaction with a carbonyl
51 oxygen in the inhibitor. In our series, docking experiments suggested that benzolactams such as **11**
52
53
54
55
56
57
58
59
60

1
2
3 and **12** (Table 1) should position their carbonyl oxygen in a similar location. Experimentally, both
4
5 benzolactams achieved a dramatic jump in inhibitory potency, with ERK2 biochemical IC₅₀ values of
6
7 11 and 24 nM respectively. The crystal structure of **11** in complex with ERK2 indicates minimal
8
9 movement of the hinge binding component, while the isoindolinone indeed positions its carbonyl
10
11 oxygen to allow a water-bridged interaction with the gatekeeper carbonyl in a similar fashion to
12
13 ulixertinib (Figure 3d). The isoindolinone carbonyl oxygen also accepts a hydrogen bond from the
14
15 side chain of Lys54, in a manner reminiscent of the binding of **4**. The isoquinolinone **12** binds
16
17 similarly to ERK2 (structure not shown); however, in view of its favourable ligand efficiency and
18
19 attractive vector towards the second pocket we chose to use the less lipophilic isoindolinone **11** as the
20
21 basis for further SAR studies.

22 23 *Growth towards the second pocket: interactions with catalytic Lys54*

24
25
26 In order to design linkers to grow from the benzolactam core of **11** towards the second pocket, we
27
28 superimposed the crystal structure of the ERK2-**11** complex onto the ERK2 structure when bound to **4**
29
30 (Figure 3e). With the Tyr36 “in” conformation, a narrow channel exists between the hinge region and
31
32 the second pocket, bounded primarily by Tyr36 and Lys54. We therefore sought to incorporate
33
34 linking groups that would be sufficiently slim to fit through this channel, and contain at least one
35
36 hydrogen bond accepting atom to interact with the Lys54 amino group. The ether analogue **13** showed
37
38 a modest increase in potency; the co-crystal structure indicated that the ether oxygen approaches the
39
40 Lys54 amino group but is positioned somewhat far for a strong hydrogen bond (O-N distance 3.4Å),
41
42 and in this co-structure Tyr36 adopts an “out” conformation (Supplementary Figure 2a). This
43
44 analogue was the first in the series to show appreciable anti-proliferative activity in BRAF^{V600E} mutant
45
46 cell lines, with IC₅₀ values of 980 and 870 nM in A375 and Colo205 96 hour proliferation assays
47
48 respectively. The morpholino analogue **14** was designed to provide an alternative hydrogen bond
49
50 acceptor to interact with Lys54; the crystal structure shows that the morpholino group does not
51
52 interact with Lys54, but rather tucks under the P-loop. This binding mode also requires a significant
53
54 twist about the C-C bond linking the pyrimidine and isoindolinone rings, which might be energetically
55
56 less favourable, consistent with the lower activity (Supplementary Figure 2b). The next series of
57

1
2
3 analogues explored the attachment of an acetamide group to the isoindolinone nitrogen. The *t*-butyl
4 amide **15** showed similar potencies to ether **13** in the biochemical and anti-proliferative assays (Table
5 1). In the ERK2 co-crystal structure of **15**, the acetamide oxygen is positioned close to the Lys54
6 amino group but again not close enough to form a strong hydrogen bond (N-O distance 3.55 Å)
7 (Figure 2f). However, in this structure Tyr36 adopts an “in” conformation, and the amide nitrogen of
8 **15** provides a synthetically accessible growth point into the second pocket, here partially filled by the
9 *t*-butyl group. The *N*-methyl tertiary amide analogue **16** shows similar biochemical and anti-
10 proliferative potencies. The ERK2 structure of **16** shows a similar binding mode to **15**, with a slight
11 shift in the positioning of the *t*-butyl group to accommodate the extra methyl group (Figure 3g).

22 23 24 *In vitro and in vivo pharmacology of early leads*

25
26 Before pursuing inhibitors extending further into the second pocket, we profiled compounds **13-16** to
27 understand the potential of this chemotype for oral exposure (Table 2). All the compounds showed
28 promising permeability in a Caco2 monolayer assay. Mouse *in vivo* pharmacokinetic experiments
29 identified the chemotype as showing low to moderate clearance with low volumes of distribution, and
30 a range of oral exposures. While the methoxyethyl derivative **13** showed low oral exposure, this was
31 significantly improved in the morpholino derivative **14**, although surprisingly the addition of the
32 weakly basic centre did not increase the volume of distribution significantly. Among the two
33 acetamido derivatives **15** and **16**, methylation of the amido NH improved oral absorption, consistent
34 with improvements in both permeability and clearance.

35
36 Since the tertiary amide **16** showed promising anti-proliferative activity and oral exposure, we carried
37 out additional pharmacological profiling (Figure 4). In BRAF^{V600E} mutant melanoma A375 cells,
38 Western blot analysis confirmed that **16** suppresses the phosphorylation of the ERK substrate RSK
39 (Figure 4a). Under these conditions **16** elicits negligible effects on ERK/pERK levels. Quantitation of
40 pRSK by Mesoscale Discovery (MSD) assay gave a cellular IC₅₀ value of 630 nM (Figure 4b). A
41 single oral 150 mg/kg dose of compound **16** administered to mice bearing sub-cutaneous colorectal
42
43
44
45
46
47
48
49
50
51
52
53
54
55
56
57
58
59
60

1
2
3 BRAF^{V600E} mutant Colo205 xenografts elicited largely complete tumor pRSK suppression at 2 and 6
4 hours, which recovered at 24 hours (Figure 4c). At the 2 and 6 hour timepoints, **16** appeared to
5 somewhat increase tumor pERK levels, possibly arising from activation of MAPK pathway feedback
6 as a result of ERK inhibition. In mice bearing sub-cutaneous Colo205 tumors, once daily oral dosing
7 of **16** at 150 mg/kg conferred significant anti-tumor activity (Figure 4d). Compound **16** was well-
8 tolerated and no excessive bodyweight loss was observed (Supplementary Figure 3a).
9
10
11
12
13
14
15
16
17

18 *Growth into the second pocket: discovery of pERK modulators*

19

20
21 With these promising results in hand, we sought to build on the favorable properties of amides **15** and
22 **16** and grow further into the second pocket to explore potential effects on pERK modulation.

23
24 Inspection of the ERK2 co-structure of **15** showed two water molecules in the cavity between the
25 inhibitor *t*-butyl group and Tyr64 (Figure 5a). Docking experiments suggested that replacement of the
26 *t*-butyl group with benzylic groups might occupy this pocket efficiently. Experimentally, the success
27 of this approach depended on the substitution at the benzylic carbon. The simple benzyl amide **17**
28 showed no potency improvement in the biochemical assay, but a significant leap in potency in the
29 antiproliferative assays (Table 3). The branched methyl (*R*)-enantiomer **18** also showed good potency
30 in both the biochemical and antiproliferative assays, while the (*S*)-enantiomer **19** was less active. The
31 dimethyl substituted analogue **20** showed intermediate activity in both biochemical and
32 antiproliferative assays. A structure of **17** was not obtained, but the structure of **18** shows the phenyl
33 group occupying the second pocket as intended (Figure 5b), while the methyl group is accommodated
34 in the space between Thr68 and Glu61 of the C- α -helix. In this structure Tyr64 adopts a slightly
35 altered conformation in which its phenol ring is twisted to engage in an edge-to-face pi-pi interaction
36 with the phenyl group of the inhibitor, forming a lid over the second pocket. Presumably the (*S*)-
37 enantiomer **19** is less active because in order to place its phenyl ring in the same position as **18**, the
38 methyl group would be eclipsed with the amide carbonyl, representing a potentially less favourable
39 inhibitor conformation. Of note, the α,α -dimethyl analogue **20** binds in a different conformation in
40
41
42
43
44
45
46
47
48
49
50
51
52
53
54
55
56
57
58
59
60

1
2
3 which the phenyl group folds back over the benzolactam core, mimicking Tyr36 in the structure of **18**,
4 while Tyr36 reverts to an “out” conformation (Figure 5c).

5
6
7 The ERK2 co-structure of α -methyl benzyl amide **18** suggested the potential for further potency gains.
8
9 At this point we used the cellular assay to drive structure-activity relationships, as highly active
10
11 compounds had a potency that exceeded the detection limit of the enzyme assay. First, although the
12
13 phenyl group is somewhat embedded in the second pocket, the 3-position is oriented towards solvent,
14
15 providing a vector for additional substitution. Introduction of a methoxy group in this position,
16
17 compound **21**, afforded a 3-4-fold increase in cellular potency, giving IC₅₀s of 37 and 33 nM in the
18
19 A375 and Colo205 antiproliferation assays respectively (Table 3). The ERK2 co-structure of **21**
20
21 shows increased surface contacts between the inhibitor methoxyphenyl group and Tyr64; in addition
22
23 the methoxyphenyl resides over the pi-cation system of Arg67 (Figure 5d). Second, inspection of the
24
25 protein environment in the vicinity of the benzylic methyl group of **18** suggested that introduction of a
26
27 hydroxyl group at this position might elicit favourable interactions with the polar sidechain of Asp167
28
29 and the backbone NH of Gly169. The corresponding (*S*)-hydroxymethyl analogue **22** showed an
30
31 approximately 3-fold increase in cellular potency compared with compound **18**, with IC₅₀s of 34 and
32
33 49 nM in the A375 and Colo205 antiproliferation assays, while the (*R*)-enantiomer is less active
34
35 (Table 3). The ERK2 co-structure of **22** shows that the hydroxyl group indeed interacts with the side
36
37 chain of Asp167 as intended, but intriguingly, the side chain of Arg67 adopts an altered conformation
38
39 to also interact with the inhibitor hydroxyl group (Figure 5e). In this way the hydroxyl group bridges a
40
41 charge-charge interaction between Asp167 and Arg67.

42
43
44 Combination of these two SAR features appeared to be additive, such that incorporation of both the 3-
45
46 methoxy group and benzylic hydroxyl in compound **24** gave high cellular potency with IC₅₀s of 7.1
47
48 and 7.3 nM in A375 and Colo205 antiproliferation assays.

49
50
51 We also explored the effects of substitution on the methylene part of the acetamide linker. Inspection
52
53 of the ERK2 co-structure of compound **22** suggested that a methyl group might be tolerated in this
54
55 position with an (*R*)-configuration to direct the substituent towards solvent. The two diastereomeric
56
57

1
2
3 analogues of **22** bearing (*R*) and (*S*) methyl groups were synthesized: the (*R*) diastereomer **25** showed
4 similar biochemical and cellular potency to **22**, while the (*S*)-diastereomer **26** was less potent,
5 possibly due to steric crowding of the methyl group with the side chain of Asp167. Although this
6 methyl group did not modulate the potency, it proved to be useful in increasing oral exposure in mice
7 as discussed below.
8
9
10
11

12
13 Combination of SAR learnings described above, including the hydroxymethyl benzyl group with a
14 methyl group on the 3-position of the phenyl ring and an (*R*)-methyl group on the acetamide linker,
15 afforded compound **27** which also showed excellent anti-proliferative potency with IC₅₀s of 4.9 and
16 7.5 nM in A375 and Colo205 cells respectively.
17
18
19
20
21

22 Several of the more potent analogues were profiled in mouse pharmacokinetic studies to assess their
23 potential for further progression into pharmacodynamic and efficacy studies (Table 2). The
24 unsubstituted benzyl analogue **17** showed good oral exposure comparable with that of the *t*-butyl
25 amide **16**. The addition of the benzylic methyl group and 3-methoxy group in **21** lowered oral
26 bioavailability, potentially due to the effect of increased lipophilicity on solubility. The
27 hydroxymethyl analogues **22**, **24**, **25** and **27** showed moderate to good bioavailability and,
28 interestingly, somewhat higher volumes of distribution which might be desirable for tumor exposure.
29
30 In this grouping the 3-methoxy substitution in **24** resulted in a significant jump in clearance, with a
31 correspondingly lower oral AUC and bioavailability than the other analogues. Compound **27**
32 possessed a promising combination of antiproliferative activity against mutant BRAF cells and oral
33 exposure in mice, and was profiled in selectivity and mechanistic cellular assays.
34
35
36
37
38
39
40
41
42
43

44 The *in vitro* activity of **27** was confirmed against both ERK1/2 isoforms: activity was close to the
45 limit of the assays, showing 60% inhibition at 1 nM and an IC₅₀ of 3.0 nM against ERK1 and ERK2
46 respectively. Screening against a panel of 429 kinases revealed excellent selectivity towards ERK1/2,
47 with only 3 kinases inhibited at >50% at 100 nM and 16 kinases at 1 μM (Supplementary Table 1). We
48 ascribe this selectivity to a number of unique features in the binding mode of compound **27** to ERK:
49 the sp³ character of the oxanyl group in the solvent exposed channel; the chloro and isoindolinone
50
51
52
53
54
55
56
57
58
59
60

1
2
3 interactions with the glutamine gatekeeper residue, present in only 2% of kinases; and the shape and
4 hydrogen bonding motifs designed to closely complement the unusual second pocket of ERK1/2.

5
6
7 In A375 cells **27** suppressed phospho levels of the downstream substrate RSK, with an IC₅₀ of 3.5 nM
8 as measured by MSD assay (Figure 6a). In addition, **27** suppressed the phosphorylation of ERK itself,
9 achieving an IC₅₀ value of 2.3 nM using ELISA (Figure 6b). Pharmacodynamic assays performed in
10 mice bearing sub-cutaneous Colo205 xenografts confirmed *in vivo* suppression of both pRSK and
11 pERK in tumors following a single 25 mg/kg oral dose of compound **27** (Figure 6c). Maximal
12 suppression of pRSK reached approximately 90% at 2 hours after dosing, while maximal suppression
13 of pERK at approximately 70% was also observed at 2 hours, both partially recovering at 6 hours and
14 completely at 24 hours.

15
16
17 Repeat oral dosing of compound **27** over 15 days elicited tumor regression in mice bearing Colo205
18 xenografts (Figure 6d). The efficacy observed in response to either once daily dosing at 50 mg/kg or
19 twice daily dosing at 25 mg/kg was very similar, suggesting that sustained suppression of ERK1/2
20 signalling may not be required for effective tumor growth inhibition. Compound **27** was well-
21 tolerated and no excessive bodyweight loss was observed (Supplementary Figure 3b).

22 23 24 *Synthesis*

25
26
27 Fragments **5** and **7-10** were synthesized in a single step from the corresponding 5-substituted 2-
28 chloropyrimidines and aminopyrazole or oxan-4-amine respectively. The isoindolinone **11** was
29 prepared according to Scheme 1. Commercial 6-bromo-2,3-dihydro-1H-isoindol-1-one **30** was
30 converted to the pinacol boronate ester **31** by palladium mediated coupling, followed by a second
31 palladium coupling to furnish the dichloropyrimidine derivative **32**, and then heating in the presence
32 of oxan-4-amine. The homologous isoquinolinone **12** required construction of the heterobicycle as
33 shown in Scheme 2. First, 2-(4-chlorophenyl)ethan-1-amine was converted to the methyl carbamate
34 **34**, which was then cyclized to give 7-chloro-1,2,3,4-tetrahydroisoquinolin-1-one (**35**) under acidic
35 conditions. Elaboration to give **12** then followed a similar process of borylation, Suzuki coupling and
36
37
38
39
40
41
42
43
44
45
46
47
48
49
50
51
52
53
54
55
56
57
58
59
60

1
2
3 chloride displacement with oxan-4-amine. In this case the more active XPhos ligand was required to
4 couple the aryl chloride **35**.

5
6
7 The N-substituted isoindolinone derivatives **13** and **14** were prepared according to Scheme 3. N-
8 Alkylation of 6-bromo-2,3-dihydro-1H-isoindol-1-one (**30**) was effected with sodium hydride and the
9 corresponding alkyl bromide, followed by sequential borylation and Suzuki coupling to give the
10 dichloropyrimidines **38** and **39**. Displacement of the 2-chloro substituent with oxan-4-amine gave the
11 final compounds **13** and **14**. The acetamide derivatives **15-24** were prepared following the general
12 procedure illustrated for compound **15** in Scheme 4. Alkylation of 6-bromo-2,3-dihydro-1H-isoindol-
13 1-one (**30**) with *t*-butyl bromoacetate followed by palladium coupling gave the boronate ester **40**,
14 which was converted to the dichloropyrimidine **41** by Suzuki coupling. Displacement of the 2-chloro
15 substituent with oxan-4-amine and cleavage of the *t*-butyl ester using anhydrous acid afforded the key
16 intermediate acid **42**. Coupling to give the final amide **15** was effected with *t*-butylamine and HBTU.
17 For other amides, alternative coupling agents were used, including HATU or T3P.
18
19
20
21
22
23
24
25
26
27
28
29

30 The synthesis of the 2-propionamide derivatives **25-27** required a modified route as outlined in
31 Scheme 5. In order to install the more bulky methylated linker, cyclization of bromomethyl
32 bromobenzoic acid **43** with alanine *t*-butyl ester was used to form the *N*-substituted lactam.
33 Conversion to the boronate ester and Suzuki coupling with trichloropyrimidine were effected as
34 previously. Attempts to install the amino-oxanyl group at this stage led to racemization of the methyl
35 group, and so the steps were reversed by first cleaving the *t*-butyl ester using TFA to give acid **47**,
36 then carrying out the amino-oxan substitution to give the intermediate **48**. Finally, amide couplings
37 using HATU or TBTU gave the final compounds **25-27**.
38
39
40
41
42
43
44
45
46
47
48

49 CONCLUSION

50
51 In recent years, fragment-based drug discovery has established a track record for providing novel start
52 points for medicinal chemistry campaigns, in some cases identifying alternative binding modes and/or
53
54
55
56
57
58
59
60

1
2
3 allosteric sites for ligand binding, and providing a rational basis for the design of drug leads and
4 candidates with carefully controlled physicochemical properties.^{29,30}
5
6

7 Here, a combined approach using X-ray crystallographic and biophysical fragment screening together
8 with structure based optimization led to the discovery of highly potent and selective orally
9 bioavailable ERK1/2 inhibitors which also block the phosphorylation of ERK1/2. Careful
10 optimization of the initial hinge binding fragment hit proved important in achieving the overall profile
11 of the lead compound. Due to the relatively large distance from the hinge to the second pocket,
12 parsimonious use of molecular weight and hydrogen bond donors was critical to balance permeability
13 with other properties in the series. The chloro substituent allowed an energetically favourable
14 interaction with the side chain carbonyl oxygen of gatekeeper Gln105 without adding a hydrogen
15 bond donor. The design of the isoindolinone core allowed a favourable interaction with the side chain
16 carbonyl of gatekeeper Gln105 bridged *via* a water molecule, while providing an optimal spatial and
17 synthetic vector with which to grow towards the second pocket. Acetamide and 2-propionamide
18 linkers provided access to the second pocket while interacting favourably with the catalytic lysine 54.
19 Finally, substituted hydroxymethyl benzyl groups provided good shape complementarity, stacking
20 and hydrogen bonding interactions with residues lining the second pocket.
21
22
23
24
25
26
27
28
29
30
31
32
33
34
35

36 Occupancy of the second pocket correlated with modulation of pERK levels, confirming the original
37 structural hypothesis. Hence, the smaller inhibitors represented by t-butyl amide **16** did not show
38 modulation of pERK levels *in vitro* or *in vivo*; while inhibitors occupying the second pocket with a
39 benzylic group, represented by compound **27**, suppressed pERK levels. The lead compound **27**
40 suppressed both pRSK and pERK1/2 in mutant BRAF cells *in vitro* and *in vivo*, and displayed
41 promising efficacy in Colo205 xenograft models. Further pharmacological characterization of **27** will
42 be published elsewhere.
43
44
45
46
47
48
49
50
51
52
53
54
55
56
57
58
59
60

EXPERIMENTAL PROCEDURES

Protein Expression, Purification & Crystallography

Full length human ERK2 (hERK2) was cloned into pET30a with a non-cleavable MAHHHHHH N-terminal tag. hERK2 was expressed in E.coli BL21(DE3) and non-phosphorylated hERK2 (confirmed by LCMS) was purified using sequential Ni-HiTRAP, desalt, Resource-Q and S75 26/60 column steps. hERK2 was crystallised under conditions adapted from Aronov et al.¹⁸ and crystals were soaked in a solution equivalent to the crystallisation solution but also containing 0.1-100 mM ligand, 10mM DTT and 10% DMSO final. Crystals were cryo-protected using crystallisation solution containing 35% 2KMPEG final. X-ray diffraction data were collected using both in-house and synchrotron X-ray sources.

ERK2 kinase assay

ERK2 kinase activity was determined using a time resolved fluorescence (TRF) activity assay. ERK2 enzyme (0.25 nM) was incubated with the substrates ATF2-GFP (0.4 μ M) and ATP (20 μ M) in 50 mM Tris pH7.5, 10 mM MgCl₂, 1 mM EGTA, 0.01% Triton X100, 1 mM DTT and 2.5% DMSO, with shaking at room temperature for 30 mins. Reactions were stopped by the addition of a stop and detection mix, containing 25 mM EDTA, 2 nM Tb-pATF2 antibody in TR-FRET dilution buffer (Life Technologies, Paisley, UK) and the plate was incubated with shaking at room temperature for 1 hour. Upon excitation at 340nm, fluorescence was measured at 520nm (A counts) and 495nm (B counts) using a Pherastar plate reader (BMG Labtech, Ortenberg, Germany).

Cell culture and reagents

The human cell lines A375 and Colo205 were purchased from the American Type Culture Collection (ATCC, Manassas, VA, USA) and the European Collection of Authenticated Cell Cultures (ECACC Salisbury, UK), respectively. The cells lines were not passaged for more than 6 months after authentication by the cell banks (DNA fingerprinting and cytogenetic analysis or short-tandem repeat (STR) PCR). Both cell lines were grown in DMEM culture medium, supplemented with 10 % FBS

(ThermoFisher Scientific, Waltham, Massachusetts, USA) and maintained at 37 °C in an atmosphere of 5 % CO₂.

Cell Proliferation Assay

Cell proliferation assays were carried out using Alamar Blue (ThermoFisher Scientific, Waltham, Massachusetts, USA) as described previously.³¹ Briefly, 5x10³ cells were seeded in complete culture medium into flat-bottomed 96-well plates, one day before the drug treatment. Cells were incubated with compound in 0.1% (v/v) dimethyl sulfoxide (DMSO) for 96 hours before viability was assessed using Alamar blue. IC₅₀ values were calculated using a sigmoidal dose response equation (Prism GraphPad software, La Jolla, CA, USA).

In vitro permeability

Permeability of test compounds was assessed using the CacoReady™ system. Test and control compounds (propranolol, antipyrine, vinblastine) were incubated at a final concentration of 10 μM in duplicate to either the apical (180 μL) of the monolayer to measure apical to basolateral transport (A>B) across the cell barrier or to the basolateral side (750 μL) to measure the basolateral to apical transport (B>A). For A>B spiking, test and control compounds were diluted from 10 mM DMSO stocks to 10 μM in HBSS buffer with 100 mM CaCl₂·2H₂O, 50 mM MgCl₂·5H₂O and 0.5 mg/mL lucifer yellow made to volume with sterile water (lucifer yellow was used to determine the integrity of the Caco-2 monolayer). For B>A compound spiking, test and control compounds were prepared as for the A>B solutions without the addition of lucifer yellow. Test and control compounds were incubated for 1 hour at 37°C in a highly humidified atmosphere of 95% air and 5% CO₂.

Western Blotting

Cells were seeded at 10⁶ cells per well, incubated overnight at 37 °C and then treated with compound for 16 hours. Cells were harvested and lysed in ice-cold Triton lysis buffer and lysates cleared by centrifugation. Colo205 xenograft tumor lysates were prepared by grinding the frozen tissue to a fine powder with a mortar/pestle under liquid nitrogen and then adding ice-cold Mesoscale Discovery

1
2
3 (MSD) lysis buffer (Rockville, Maryland, USA). Samples were freeze-thawed, vortexed and then
4 lysates cleared by centrifugation. Protein concentrations were determined using a BCA protein assay
5 (ThermoFisher Scientific, Waltham, Massachusetts, USA). Equivalent amounts of protein lysates
6 were resolved by SDS PAGE Tris-Glycine gel systems, transferred to nitrocellulose membranes and
7 incubated with primary antibodies specific for phospho-p90RSK (Thr359), phospho-p42/44 MAPK
8 (ERK1/2), p44/42 MAPK (ERK1/2) (Cell Signaling Technology, Massachusetts, USA), RSK (R&D
9 Systems, Minneapolis, USA), and actin (Abcam, Cambridge, UK). Blots were then incubated with
10 infrared-dye-labeled secondary antibodies and detected on the Odyssey infrared imaging system
11 (LiCor Bioscience, Lincoln, USA).

21 **Quantification of pRSK by MSD**

22
23 A375 cells were seeded at 1.5×10^4 cells per well into 96-well plates and allowed to recover for 16 h,
24 prior to the addition of compounds (in 0.1% DMSO v/v) and incubation for a further 4 h. Cells were
25 lysed by adding cell lysis buffer (Cell Signaling Technology, Massachusetts, USA) and incubating at
26 room temperature for 20 minutes. Custom MSD plates (Meso Scale Discovery, Maryland, USA) pre-
27 coated with anti-pRSK antibody (Cell Signaling Technology, Massachusetts, USA) were blocked with
28 kit blocking buffer for 1 hour at room temperature, prior to washing. Equivalent amounts of protein
29 lysate were added to the blocked plates and incubated for 3 hours at room temperature. After washing,
30 plates were incubated for 1 hour at room temperature with sulfo-tag conjugated anti-RSK detection
31 antibodies (R&D Systems, Minneapolis, USA). Plates were washed, and read buffer added before
32 reading the plate on a MESO QuickPlex SQ 120 (Meso Scale Discovery, Maryland, USA). IC_{50}
33 values were calculated using a sigmoidal dose response equation (Prism GraphPad software, La Jolla,
34 CA, USA). For pharmacodynamic studies, Colo205 xenograft tumor lysates were prepared as
35 described above, and transferred directly to Custom MSD pRSK plates (Meso Scale Discovery,
36 Maryland, USA) for analysis.

51 **Quantification of pERK by ELISA**

52
53 A375 cells were treated with compounds and lysed as described above. Lysates were then cleared by
54 centrifugation, transferred to pERK ELISA plates (Cell Signalling technology, Massachusetts, USA)

1
2
3 and analysed according to manufacturer's instructions. IC₅₀ values were calculated using a sigmoidal
4 dose response equation (Prism GraphPad software, La Jolla, CA, USA). For pharmacodynamic
5 studies, Colo205 xenograft tumor lysates were prepared as described above, transferred to pERK
6
7 ELISA plates (Cell Signalling technology, Massachusetts, USA) and analysed according to
8
9 manufacturer's instructions.
10
11

12 13 ***In vivo* studies**

14
15
16 The care and treatment of experimental animals were in accordance with the United Kingdom
17 Coordinating Committee for Cancer Research guidelines³² and the United Kingdom Animals
18 (Scientific Procedures) Act 1986.³³ Mouse studies were performed with mice allowed access to food
19
20 and water ad libitum.
21
22
23

24 25 **Pharmacokinetic studies**

26
27 For intravenous administrations, test compounds were formulated in either 20% DMA/80% saline,
28 10% DMSO/20% PEG400/70% water or 10% DMSO/90% saline. For oral administrations test
29
30 compounds were formulated in either 10% ethanol/10% cremaphor/10% PEG200/70% water, 20%
31
32 PEG400/80% HPMC or 10% DMSO/20% cremaphor/70% saline. Intravenous dosing at 0.5 mg/kg
33
34 was administered via the lateral tail vein at a dose volume of 5 mL/kg. Test compounds were
35
36 administered orally at 5 mg/kg by nasogastric gavage at a dose volume of 10 mL/kg. All doses were
37
38 calculated as freebase equivalent per kg of bodyweight. Pharmacokinetic studies were performed in
39
40 male Balb/c mice, obtained from Harlan Laboratories Inc. (Shardlow, UK). Following dosing in
41
42 mice, blood samples (0.2 mL) were drawn in tubes containing potassium EDTA, via either saphenous
43
44 vein bleeding or cardiac puncture at various time points over 24 hours using sparse sampling (n=3 per
45
46 time point), prior to centrifugation (2000 g at 4°C, 10 min). The resultant plasma was separated from
47
48 the erythrocyte pellets for analysis and stored at -20°C. Terminal samples were collected via cardiac
49
50 puncture and centrifuged (10 000 g at 4°C, 2 min) and the resultant plasma stored at -20°C. Non-
51
52 compartmental pharmacokinetic (PK) analyses were performed using Phoenix 6.3.0.395® (Certara
53
54 USA, Inc.) software. Calculated parameters included clearance, volume of distribution (V_{ss}), time of
55
56
57
58
59
60

1
2
3 maximum observed concentration (T_{max}), maximum concentration (C_{max}), terminal half-life, area
4 under the curve (AUC) from the time of dosing to the last measurable concentration (AUC_{last}) and
5 extrapolated to infinity ($AUC_{0-\infty}$). Non-compartmental PK fitting to sparse sampling data allowed
6 the calculation of standard errors on AUC_{last} and C_{max} .
7
8
9

10 11 **Xenograft Studies**

12
13 Colo205 xenografts were prepared by subcutaneously injecting 5×10^6 cells suspended in serum-free
14 medium mixed 1:1 with Matrigel (BD Biosciences, San Jose, CA, USA) into the right flank of each
15 male BALB/c nude mouse. Tumors were measured using caliper and tumour volumes calculated by
16 applying the formula for an ellipsoid. For efficacy studies, when the tumours reached an average of
17 approximately 200 mm^3 , mice were randomised into groups of 8. Mice were dosed orally once a day
18 at a dose of 150 mg/kg of compound **16** and either once a day with 50 mg/kg or twice a day with 25
19 mg/kg of compound **27**. Body weights were recorded daily and tumor volumes were measured every
20 3–4 days. For PKPD studies, a single dose of compound was administered orally to mice. Following
21 dosing, blood samples were drawn in tubes containing potassium EDTA via either saphenous vein
22 bleeding or cardiac puncture at various time points, prior to centrifugation ($2000g$ at 4°C , 10 min).
23 The resultant plasma was separated from the erythrocyte pellets for analysis and stored at -20°C .
24
25 Tumors were immediately excised and flash-frozen in liquid nitrogen.
26
27
28
29
30
31
32
33
34
35
36
37

38 **Bioanalysis**

39
40 All *in vitro* and *in vivo* samples were extracted by protein precipitation with acetonitrile containing
41 internal standard (1:3 v/v). For quantitative studies, calibration standards and quality controls were
42 prepared in blank matrix and extracted under the same conditions. All samples were centrifuged at
43 3700 rpm at 4°C for 20 min. Compound bioanalysis of all *in vitro* and *in vivo* samples were
44 performed using high performance liquid chromatography mass spectrometry (LC/MS). Test
45 compounds and the internal standard were ionised using positive mode (ESI+) electrospray ionisation.
46
47 Analytes were detected using multiple reaction monitoring (MRM). Test compounds typically ran on
48 a gradient HPLC method over 5 min with a 10 mM ammonium acetate and acetonitrile mobile phase
49
50
51
52
53
54
55
56
57
58
59
60

1
2
3 at a flow rate of 0.5 mL/min. Separation was typically achieved using an Acquity HSS T3 1.8 μ M
4
5 50x2.1 mm column maintained at 40°C.
6

7 **Synthesis of Compound 27 and intermediates 44-48**

8
9
10 **General procedures:** All solvents and commercially available reagents were used as
11 received. All reactions were followed by TLC analysis (TLC plates GF254, Merck) or LC-
12 MS (liquid chromatography mass spectrometry). LC-MS analysis was performed with an
13
14 Agilent or Shimadzu LC system with variable wavelength UV detection using reverse phase
15 chromatography with a CH₃CN and water gradient with a 0.02 or 0.1% TFA modifier (added
16 to each solvent) and using a reverse phase column, e.g., Thermo Hypersil Gold C18. MS was
17 determined using either PE Sciex 150EX LC-MS, Waters ZQ LC-MS, or Agilent 6140 LC-
18 MS Single Quadrupole instruments. Column chromatography was performed on prepacked
19 silica gel columns (3090 mesh, IST) using a Biotage SP4 or similar. NMR spectra are
20 referenced as follows: ¹H (400 MHz), internal standard TMS at δ = 0.00. Abbreviations for
21 multiplicities observed in NMR spectra: s; singlet; br s, broad singlet; d, doublet; t, triplet; q,
22 quadruplet; p, pentuplet; spt, septuplet; m, multiplet. All compounds reported are of at least
23 95% purity according to LC-MS unless stated otherwise.
24
25
26
27
28
29
30
31
32
33
34
35
36
37
38
39
40
41

42 **(2R)-2-(6-{5-Chloro-2-[(oxan-4-yl)amino]pyrimidin-4-yl}-1-oxo-2,3-dihydro-1H- 43 isoindol-2-yl)-N-[(1S)-2-hydroxy-1-(3-methylphenyl)ethyl]propanamide (27)**

44
45 Triethylamine (2.060 mL, 14.78 mmol) was added to a stirred suspension of (R)-2-(6-(5-
46 chloro-2-((oxan-4-yl)amino)pyrimidin-4-yl)-1-oxoisoindolin-2-yl)propanoic acid (1.54 g,
47 3.69 mmol) and (S)-2-amino-2-(3-tolyl)ethanol hydrochloride (0.763 g, 4.06 mmol) in DMF
48 (15 mL, 194 mmol). After 15 minutes, TBTU (1.305 g, 4.06 mmol) was added and the
49 mixture was stirred for 2 h at room temperature. The reaction was diluted with EtOAc (30
50
51
52
53
54
55
56
57

mL) and water (100 mL). The phases were separated and the aqueous phase was extracted with EtOAc (2x30 mL). The combined organic extracts were washed with NH₄Cl (100 mL), NaHCO₃ (100 mL), brine (2x100 mL), dried (MgSO₄) and concentrated. The crude product was purified by chromatography (SiO₂, 40 g column, 0-7% MeOH in DCM) to afford the product as a colourless gum. The gum was triturated with diethyl ether (100 mL) to give the title compound as a colourless solid (1.409 g, 68%).

¹H NMR (DMSO-*d*₆) 8.52 (d, *J* = 8.1 Hz, 1H), 8.44 (s, 1H), 8.04 (d, *J* = 1.5 Hz, 1H), 7.97 (dd, *J* = 7.9, 1.7 Hz, 1H), 7.74 (d, *J* = 7.9 Hz, 1H), 7.67–7.50 (m, 1H), 7.20 (t, *J* = 7.5 Hz, 1H), 7.12–7.07 (m, 2H), 7.04 (d, *J* = 7.5 Hz, 1H), 5.00 (q, *J* = 7.2 Hz, 1H), 4.84 (t, *J* = 5.5 Hz, 1H), 4.82–4.71 (m, 2H), 4.59 (d, *J* = 18.1 Hz, 1H), 3.98–3.81 (m, 3H), 3.60–3.49 (m, 2H), 3.43–3.32 (m, 2H), 2.29 (s, 3H), 1.92–1.80 (m, 2H), 1.61–1.46 (m, 2H), 1.43 (d, *J* = 7.2 Hz, 3H).

¹³C NMR (DMSO-*d*₆) 170.67, 166.85, 161.40 (broad), 159.99, 158.10 (broad), 143.89, 140.99, 137.05, 135.92 (broad), 132.06, 131.97, 128.00, 127.44, 127.40, 123.79, 123.39, 123.12, 114.67, 65.99, 64.55, 55.19, 49.58, 47.15, 47.07, 32.27, 21.07, 16.28.

HRMS (ESI-QTOF): *m/z* [M+H]⁺ Calcd for C₂₉H₃₂ClN₅O₄ 550.2213; Found 550.2205. Δ = -1.46 ppm.

***tert*-Butyl (2*R*)-2-(6-bromo-1-oxo-2,3-dihydro-1*H*-isoindol-2-yl)propanoate (44)**

DIPEA (28.5 ml, 163 mmol) and (*R*)-*tert*-butyl 2-aminopropanoate hydrochloride (14.83 g, 82 mmol) were added to a stirred solution of methyl 5-bromo-2-(bromomethyl)benzoate (16.76 g, 54.4 mmol) in MeCN (100 ml) under nitrogen and the mixture stirred and heated to 75 °C for 24 h. The solvent was removed *in vacuo* and the residue partitioned between Et₂O (500 mL) and 10% aqueous citric acid (200 ml). The organic phase was collected and washed

1
2
3 with water (200 ml) followed by sat.NaHCO₃ (100 ml). The ethereal solution was dried
4 (MgSO₄), filtered and concentrated to a solid. The solid was slurried with isohexane (200 ml)
5 and collected by filtration to afford the title compound as a cream coloured solid (15.25 g,
6
7 44.8 mmol, 82%). ¹H NMR (CDCl₃): 8.00 (d, 1H), 7.66 (dd, 1H), 7.34 (dd, 1H), 5.07 (q,
8
9 1H), 4.60 (d, 1H), 4.35 (d, 1H), 1.54 (d, 3H), 1.44 (s, 9H). LC-MS: [M+H-tBu]⁺ = 284/286.
10
11
12
13
14
15
16

17 ***tert*-Butyl (2*R*)-2-[1-oxo-6-(4,4,5,5-tetramethyl-1,3,2-dioxaborolan-2-yl)-2,3-dihydro-1H-**
18 **isoindol-2-yl]propanoate (45)**
19
20

21
22 A 25 mL round bottom flask was charged with (*R*)-*tert*-butyl 2-(6-bromo-1-oxoisoindolin-2-
23 yl)propanoate (9 g, 26.5 mmol), bis(pinacolato)diboron (8.06 g, 31.7 mmol), potassium
24 acetate (7.79 g, 79 mmol) and XPhos Pd G3 (0.448 g, 0.529 mmol). The system was
25 evacuated and back-filled with nitrogen (x 4). Dioxane (70 mL) was added and the
26 evacuation/back-filling procedure repeated (x 4). The reaction was heated to 90 °C and stirred
27 under nitrogen for 2h. After cooling to room temperature, the reaction was diluted with
28 EtOAc (10 mL) and filtered through Celite. The filtrate was concentrated *in vacuo* to give the
29 crude product as a pale brown solid. The crude product was purified by chromatography
30 (SiO₂, 80 g column, 0-50% EtOAc in iso-hexane) to afford the title compound as an off white
31 solid (9.6 g, 94%). ¹H NMR (DMSO-d₆): 7.95 (s, 1H), 7.89 (dd, 1H), 7.64 (dd, 1H), 4.79 (q,
32
33 1H), 4.57 (d, 1H), 4.50 (d, 1H), 1.48 (d, 3H), 1.38 (s, 9H), 1.31 (s, 12H). LCMS: [M+H]⁺ =
34
35 332.
36
37
38
39
40
41
42
43
44
45
46
47
48
49
50
51

52 ***tert*-Butyl (2*R*)-2-[6-(2,5-dichloropyrimidin-4-yl)-1-oxo-2,3-dihydro-1H-isoindol-2-**
53 **yl]propanoate (46)**
54
55
56
57
58
59
60

1
2
3 A mixture of (*R*)-*tert*-butyl 2-(1-oxo-6-(4,4,5,5-tetramethyl-1,3,2-dioxaborolan-2-
4 yl)isoindolin-2-yl)propanoate (5.0 g, 12.78 mmol), 2,4,5-trichloropyrimidine (3.52 g, 19.17
5 mmol) and 2.0 M Na₂CO₃ (aq.) (12.78 ml, 25.6 mmol) in dioxane (64 mL) was evacuated
6 and back-filled with nitrogen (x 3). Pd(PPh₃)₄ (0.738 g, 0.639 mmol) was added and the
7 system was evacuated and back-filled with nitrogen (x 3). The mixture was heated to 90 °C
8 and stirred for 6 h under nitrogen. The reaction was diluted with water (150 mL) and EtOAc
9 (150 mL). The phases were separated and the aqueous phase was extracted with EtOAc (2 x
10 120 mL). The combined organic extracts were washed with brine (200 mL), dried (MgSO₄)
11 and concentrated. The crude product was adsorbed onto silica and purified by
12 chromatography (SiO₂, 220 g column, 0-30% EtOAc/isohexane) to afford (*R*)-*tert*-butyl 2-(6-
13 (2,5-dichloropyrimidin-4-yl)-1-oxoisoindolin-2-yl)propanoate as an off white solid (4.204 g,
14 77 %). ¹H NMR (DMSO-d₆): 9.03 (s, 1H), 8.14 (d, 1H), 8.06 (dd, 1H), 7.83 (dd, 1H), 4.82
15 (q, 1H), 4.67 (d, 1H), 4.62 (s, 1H), 1.51 (d, 3H), 1.40 (s, 9H). LCMS: [M+Na]⁺ = 430.
16
17
18
19
20
21
22
23
24
25
26
27
28
29
30
31
32
33

34 **(*R*)-2-(6-(2,5-Dichloropyrimidin-4-yl)-1-oxoisoindolin-2-yl)propanoic acid**

35 **trifluoroacetic acid salt (47)**

36
37
38
39 Trifluoroacetic acid (25 ml, 324 mmol) was added dropwise to a solution of *tert*-butyl (2*R*)-2-
40 [6-(2,5-dichloropyrimidin-4-yl)-1-oxo-2,3-dihydro-1*H*-isoindol-2-yl]propanoate (4.5 g, 11.02
41 mmol) in DCM (25 ml) and the mixture was stirred at room temperature for 1 h. The mixture
42 was concentrated *in vacuo* and azeotroped with toluene (3x50 ml). The solid was stirred and
43 sonicated in Et₂O and collected by filtration, washing with Et₂O. The solid was air dried
44 overnight to afford the title compound as a colourless solid (3.7g, 95%). The product was
45 used without further purification. ¹H NMR (DMSO-d₆): 12.99 (s, 1H), 9.04 (s, 1H), 8.13 (dd,
46
47
48
49
50
51
52
53
54
55
56
57
58
59
60

1
2
3 1H), 8.06 (dd, 1H), 7.83 (dd, 1H), 4.87 (q, 1H), 4.67 (d, 1H), 4.61 (d, 1H), 1.54 (d, 3H). LC-
4
5 MS: [M+H]⁺ = 352.
6
7
8
9

10
11 **(R)-2-(6-{5-Chloro-2-[(oxan-4-yl)amino]pyrimidin-4-yl}-1-oxisoindolin-2-yl)propanoic**
12
13 **acid (48)**
14

15
16 (R)-2-(6-(2,5-Dichloropyrimidin-4-yl)-1-oxisoindolin-2-yl)propanoic acid (20g, 56.8
17
18 mmol), oxan-4-amine HCl (23.4g, 0.17mol, 3eq) and potassium hydroxide (2M aq., 114ml,
19
20 0.227mol, 4eq) were charged to a reaction vessel with stirring. Heat was applied to 90°C for
21
22 19hrs. The reaction was cooled and hydrochloric acid (2M aq., 57ml) was added, causing the
23
24 immediate formation of a thick colourless precipitate. The slurry was filtered, and the filter
25
26 cake washed with water (50ml), then petrol (100ml, 200ml). The resulting solid was dried
27
28 under vacuum at 40°C to give the title compound as an off white solid (24.6g, quant.).
29

30
31
32 1H NMR (DMSO-d₆): 12.95 (1H, br. s), 8.45 (1H, s), 8.03 (1H, s), 7.99 (1H, dd), 7.91 (1H,
33
34 br. s), 7.76 (1H, d), 7.60 (1H, s), 4.87 (1H, q), 4.61 (2H, dd), 3.99-3.80 (3H, m), 1.85 (2H, d),
35
36 1.61-1.45 (3H, m), 1.53 (3H, d). 1H obscured by solvent peaks.
37
38
39
40
41
42
43
44
45
46
47
48
49
50
51
52
53
54
55
56
57
58
59
60

AUTHOR INFORMATION**Corresponding Author**

*T.D.H. Tel: +44 (0) 1223 226270. Fax: +44 (0) 1223 226201. Email:
Tom.Heightman@astx.com

ACKNOWLEDGEMENTS

The authors wish to thank Dr Anne Cleasby for assistance in the refinement of X-ray crystal structures, Mr Torren Peakman for confirmation of NMR assignments and Mr Stuart Whibley for assistance in the LC-MS characterization and purification of compounds.

ABBREVIATIONS

BRAF, B-Raf proto-oncogene; DSF, differential scanning fluorimetry; ERK, extracellular signal-related kinase; HATU, 1-[bis(dimethylamino)methylene]-1H-1,2,3-triazolo[4,5-b]pyridinium 3-oxid hexafluorophosphate; HBSS, Hanks' Balanced Salt Solution; HBTU, N,N,N',N'-tetramethyl-O-(1H-benzotriazol-1-yl)uronium hexafluorophosphate; HPMC, hydroxypropyl methylcellulose; MAPK, mitogen-activated protein kinase; MEK, mitogen activated protein kinase kinase; MSD, meso scale discovery; RAS, retrovirus associated DNA sequence; RSK, ribosomal S6 kinase; T3P, 2,4,6-tripropyl-1,3,5,2,4,6-trioxatriphosphorinane-2,4,6-trioxide; TBTU, 2-(1H-benzotriazole-1-yl)-1,1,3,3-tetramethyluronium tetrafluoroborate; TRF, time-resolved fluorescence.

ASSOCIATED CONTENT*PDB ID Codes*

Coordinates and structure factors for the ERK2-ligand complex have been deposited with PDB with the following accession codes: **1**, 6gdq; **4**, 6gdm; **5**, 6g92; **6**, 6g8x; **10**, 6g91; **11**, 6g93; **13**, 6g97; **14**, 6g9a; **15**, 6g9d; **16**, 6g9h; **18**, 6g9j; **20**, 6g9m; **21**, 6geo; **22**, 6g9k; **27**, 6g9n. Authors will release the atomic coordinates and experimental data upon article publication.

SUPPORTING INFORMATION

The following Figures and Tables are provided as Supporting Information: S2 – Supplementary Figure 1 – Structure of ERK1/2 inhibitor Vertex 11e. S3 – Supplementary Figure 2 - ERK2 co-structures of methoxyethyl analogue **13** and morpholinoethyl analogue **14**. S4 – Supplementary Figure 3 - Effects of compound treatment on the body weight of mice bearing Colo205 tumor xenografts. S5 – Supplementary Table 1 - Kinome selectivity profile of Compound **27**. S6 – Additional synthetic procedures for compounds **5-26** and associated intermediates. Molecular formula strings are provided as a csv file.

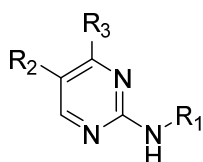
REFERENCES

1. Roskoski Jr, R. ERK1/2 MAP Kinases: Structure, Function, and Regulation. *Pharmacological Research* **2012**, *66* (2), 105-143.
2. Prior, I. A.; Lewis, P. D.; Mattos, C. A Comprehensive Survey of Ras Mutations in Cancer. *Cancer Research* **2012**, *72* (10), 2457-2467.
3. Caunt, C. J.; Sale, M. J.; Smith, P. D.; Cook, S. J. MEK1 and MEK2 Inhibitors and Cancer Therapy: the Long and Winding Road. *Nat Rev Cancer* **2015**, *15* (10), 577-592.
4. Corcoran, R. B.; Settleman, J.; Engelman, J. A. Potential Therapeutic Strategies to Overcome Acquired Resistance to BRAF or MEK Inhibitors in BRAF Mutant Cancers. *Oncotarget* **2011**, *2* (4), 336-346.
5. Little, A. S.; Smith, P. D.; Cook, S. J. Mechanisms of Acquired Resistance to ERK1/2 Pathway Inhibitors. *Oncogene* **2012**, *32*, 1207.
6. Lloyd, A. C. Distinct Functions for ERKs? *Journal of Biology* **2006**, *5* (5), 13.
7. Qin, J.; Xin, H.; Nickoloff, B. J. Specifically Targeting ERK1 or ERK2 Kills Melanoma Cells. *Journal of Translational Medicine* **2012**, *10* (1), 15.
8. Shin, M.; Franks, C. E.; Hsu, K.-L. Isoform-Selective Activity-Based Profiling of ERK Signaling. *Chemical Science* **2018**, *9* (9), 2419-2431.
9. Lefloch, R.; Pouysségur, J.; Lenormand, P. Single and Combined Silencing of ERK1 and ERK2 Reveals Their Positive Contribution to Growth Signaling Depending on Their Expression Levels. *Molecular and Cellular Biology* **2008**, *28* (1), 511-527.
10. Rodríguez, J.; Crespo, P. Working Without Kinase Activity: Phosphotransfer-Independent Functions of Extracellular Signal-Regulated Kinases. *Science Signaling* **2011**, *4* (196), re3.
11. Germann, U.; Furey, B.; Roix, J.; Markland, W.; Hoover, R.; Aronov, A.; Hale, M.; Chen, G.; Martinez-Botella, G.; Alargova, R.; Fan, B.; Sorrell, D.; Meshaw, K.; Shapiro, P.; Wick, M. J.; Benes, C.; Garnett, M.; DeCrescenzo, G.; Namchuk, M.; Saha, S.; Welsch, D. J. Abstract 4693: The Selective ERK Inhibitor BVD-523 is Active in Models of MAPK Pathway-Dependent Cancers, Including Those with Intrinsic and Acquired Drug Resistance. *Cancer Research* **2015**, *75* (15 Supplement), 4693-4693.
12. Blake, J. F.; Burkard, M.; Chan, J.; Chen, H.; Chou, K.-J.; Diaz, D.; Dudley, D. A.; Gaudino, J. J.; Gould, S. E.; Grina, J.; Hunsaker, T.; Liu, L.; Martinson, M.; Moreno, D.; Mueller, L.; Orr, C.; Pacheco, P.; Qin, A.; Rasor, K.; Ren, L.; Robarge, K.; Shahidi-Latham, S.; Stults, J.; Sullivan, F.; Wang, W.; Yin, J.; Zhou, A.; Belvin, M.; Merchant, M.; Moffat, J.; Schwarz, J. B. Discovery of (S)-1-(1-(4-Chloro-3-fluorophenyl)-2-hydroxyethyl)-4-(2-((1-methyl-1H-pyrazol-5-yl)amino)pyrimidin-4-yl)pyridin-2(1H)-one (GDC-0994), an Extracellular Signal-Regulated Kinase 1/2 (ERK1/2) Inhibitor in Early Clinical Development. *Journal of Medicinal Chemistry* **2016**, *59* (12), 5650-5660.
13. Study of MK-8353 in Combination With Pembrolizumab (MK-3475) in Participants With Advanced Malignancies (MK-8353-013). www.clintrials.gov NCT02972034, April 26th, 2017.
14. A Study of LY3214996 Administered Alone or in Combination With Other Agents in Participants With Advanced/Metastatic Cancer. www.clintrials.gov NCT02857270, April 26th, 2017.
15. A Phase I Clinical Study With Investigational Compound LTT462 in Adult Patients With Specific Advanced Cancers. www.clintrials.gov NCT02711345, April 26th, 2017.
16. First-in-Human Study of KO-947 in Non-Hematological Malignancies. www.clintrials.gov NCT03051035, April 26th, 2017.
17. Aronov, A. M.; Baker, C.; Bemis, G. W.; Cao, J.; Chen, G.; Ford, P. J.; Germann, U. A.; Green, J.; Hale, M. R.; Jacobs, M.; Janetka, J. W.; Maltais, F.; Martinez-Botella, G.; Namchuk, M. N.; Straub, J.; Tang, Q.; Xie, X. Flipped Out: Structure-Guided Design of Selective Pyrazolopyrrole ERK Inhibitors. *Journal of Medicinal Chemistry* **2007**, *50* (6), 1280-1287.
18. Aronov, A. M.; Tang, Q.; Martinez-Botella, G.; Bemis, G. W.; Cao, J.; Chen, G.; Ewing, N. P.; Ford, P. J.; Germann, U. A.; Green, J.; Hale, M. R.; Jacobs, M.; Janetka, J. W.; Maltais, F.; Markland, W.; Namchuk, M. N.; Nanthakumar, S.; Poondru, S.; Straub, J.; ter Haar, E.; Xie, X. Structure-Guided Design of Potent and Selective Pyrimidylpyrrole Inhibitors of Extracellular Signal-Regulated Kinase (ERK) Using Conformational Control. *Journal of Medicinal Chemistry* **2009**, *52* (20), 6362-6368.

19. Deng, Y.; Shipps, G. W.; Cooper, A.; English, J. M.; Annis, D. A.; Carr, D.; Nan, Y.; Wang, T.; Zhu, H. Y.; Chuang, C.-C.; Dayananth, P.; Hruza, A. W.; Xiao, L.; Jin, W.; Kirschmeier, P.; Windsor, W. T.; Samatar, A. A. Discovery of Novel, Dual Mechanism ERK Inhibitors by Affinity Selection Screening of an Inactive Kinase. *Journal of Medicinal Chemistry* **2014**, *57* (21), 8817-8826.
20. Bagdanoff, J. T.; Jain, R.; Han, W.; Zhu, S.; Madiera, A.-M.; Lee, P. S.; Ma, X.; Poon, D. Tetrahydropyrrolo-diazepenones as Inhibitors of ERK2 Kinase. *Bioorganic & Medicinal Chemistry Letters* **2015**, *25* (18), 3788-3792.
21. Lim, J.; Kelley, E. H.; Methot, J. L.; Zhou, H.; Petrocchi, A.; Chen, H.; Hill, S. E.; Hinton, M. C.; Hruza, A.; Jung, J. O.; Maclean, J. K. F.; Mansueto, M.; Naumov, G. N.; Philippar, U.; Raut, S.; Spacciopoli, P.; Sun, D.; Siliphaivanh, P. Discovery of 1-(1H-Pyrazolo[4,3-c]pyridin-6-yl)urea Inhibitors of Extracellular Signal-Regulated Kinase (ERK) for the Treatment of Cancers. *Journal of Medicinal Chemistry* **2016**, *59* (13), 6501-6511.
22. Lechtenberg, B. C.; Mace, P. D.; Sessions, E. H.; Williamson, R.; Stalder, R.; Wallez, Y.; Roth, G. P.; Riedl, S. J.; Pasquale, E. B. Structure-Guided Strategy for the Development of Potent Bivalent ERK Inhibitors. *ACS Medicinal Chemistry Letters* **2017**, *8* (7), 726-731.
23. Ward, R. A.; Bethel, P.; Cook, C.; Davies, E.; Debreczeni, J. E.; Fairley, G.; Feron, L.; Flemington, V.; Graham, M. A.; Greenwood, R.; Griffin, N.; Hanson, L.; Hopcroft, P.; Howard, T. D.; Hudson, J.; James, M.; Jones, C. D.; Jones, C. R.; Lamont, S.; Lewis, R.; Lindsay, N.; Roberts, K.; Simpson, I.; St-Gallay, S.; Swallow, S.; Tang, J.; Tonge, M.; Wang, Z.; Zhai, B. Structure-Guided Discovery of Potent and Selective Inhibitors of ERK1/2 from a Modestly Active and Promiscuous Chemical Start Point. *Journal of Medicinal Chemistry* **2017**, *60* (8), 3438-3450.
24. Li, B. T.; Janku, F.; Patel, M. R.; Sullivan, R. J.; Flaherty, K.; Buchbinder, E. I.; Lacouture, M. E.; Varghese, A. M.; Wong, D. J. L.; Sznol, M.; Sosman, J. A.; Keedy, V. L.; Wang-Gillam, A.; Ribas, A.; Tolcher, A. W.; Patel, S. P.; Varterasian, M. L.; Welsch, D.; Hyman, D. M.; Infante, J. R. First-in-Class Oral ERK1/2 Inhibitor Ulixertinib (BVD-523) in Patients with Advanced Solid Tumors: Final Results of a Phase I Dose Escalation and Expansion Study. *Journal of Clinical Oncology* **2017**, *35* (15_suppl), 2508-2508.
25. Moschos, S. J.; Sullivan, R. J.; Hwu, W.-J.; Ramanathan, R. K.; Adjei, A. A.; Fong, P. C.; Shapira-Frommer, R.; Tawbi, H. A.; Rubino, J.; Rush, T. S., III; Zhang, D.; Miselis, N. R.; Samatar, A. A.; Chun, P.; Rubin, E. H.; Schiller, J.; Long, B. J.; Dayananth, P.; Carr, D.; Kirschmeier, P.; Bishop, W. R.; Deng, Y.; Cooper, A.; Shipps, G. W.; Moreno, B. H.; Robert, L.; Ribas, A.; Flaherty, K. T. Development of MK-8353, an Orally Administered ERK1/2 Inhibitor, in Patients with Advanced Solid Tumors. *JCI Insight* **2018**, *3* (4).
26. Morris, E. J.; Jha, S.; Restaino, C. R.; Dayananth, P.; Zhu, H.; Cooper, A.; Carr, D.; Deng, Y.; Jin, W.; Black, S.; Long, B.; Liu, J.; DiNunzio, E.; Windsor, W.; Zhang, R.; Zhao, S.; Angagaw, M. H.; Pinheiro, E. M.; Desai, J.; Xiao, L.; Shipps, G.; Hruza, A.; Wang, J.; Kelly, J.; Paliwal, S.; Gao, X.; Babu, B. S.; Zhu, L.; Daublain, P.; Zhang, L.; Lutterbach, B. A.; Pelletier, M. R.; Philippar, U.; Siliphaivanh, P.; Witter, D.; Kirschmeier, P.; Bishop, W. R.; Hicklin, D.; Gilliland, D. G.; Jayaraman, L.; Zawal, L.; Fawell, S.; Samatar, A. A. Discovery of a Novel ERK Inhibitor with Activity in Models of Acquired Resistance to BRAF and MEK Inhibitors. *Cancer Discovery* **2013**, *3* (7), 742-750.
27. Chaikwad, A.; M C Tacconi, E.; Zimmer, J.; Liang, Y.; Gray, N. S.; Tarsounas, M.; Knapp, S. A Unique Inhibitor Binding Site in ERK1/2 is Associated with Slow Binding Kinetics. *Nat Chem Biol* **2014**, *10* (10), 853-860.
28. Rudolph, J.; Xiao, Y.; Pardi, A.; Ahn, N. G. Slow Inhibition and Conformation Selective Properties of Extracellular Signal-Regulated Kinase 1 and 2 Inhibitors. *Biochemistry* **2015**, *54* (1), 22-31.
29. Erlanson, D. A.; Fesik, S. W.; Hubbard, R. E.; Jahnke, W.; Jhoti, H. Twenty Years On: The Impact of Fragments on Drug Discovery. *Nature Reviews Drug Discovery* **2016**, *15*, 605.
30. Johnson, C. N.; Erlanson, D. A.; Jahnke, W.; Mortenson, P. N.; Rees, D. C. Fragment-to-Lead Medicinal Chemistry Publications in 2016. *Journal of Medicinal Chemistry* **2018**, *61* (5), 1774-1784.
31. Squires, M. S.; Feltell, R. E.; Wallis, N. G.; Lewis, E. J.; Smith, D.-M.; Cross, D. M.; Lyons, J. F.; Thompson, N. T. Biological Characterization of AT7519, a Small-Molecule Inhibitor of Cyclin-Dependent Kinases, in Human Tumor Cell Lines. *Molecular Cancer Therapeutics* **2009**, *8* (2), 324-332.

- 1
2
3 32. Workman, P.; Aboagye, E. O.; Balkwill, F.; Balmain, A.; Bruder, G.; Chaplin, D. J.; Double,
4 J. A.; Everitt, J.; Farningham, D. A. H.; Glennie, M. J.; Kelland, L. R.; Robinson, V.; Stratford, I. J.;
5 Tozer, G. M.; Watson, S.; Wedge, S. R.; Eccles, S. A. An Ad Hoc Committee of the National Cancer
6 Research, I., Guidelines for the Welfare and Use of Animals in Cancer Research. *British Journal Of*
7 *Cancer* **2010**, *102*, 1555.
8 33. Hollands, C. The Animals (Scientific Procedures) Act 1986. *The Lancet* **1986**, *328* (8497),
9 32-33.
10
11
12
13
14
15
16
17
18
19
20
21
22
23
24
25
26
27
28
29
30
31
32
33
34
35
36
37
38
39
40
41
42
43
44
45
46
47
48
49
50
51
52
53
54
55
56
57
58
59
60

TABLES

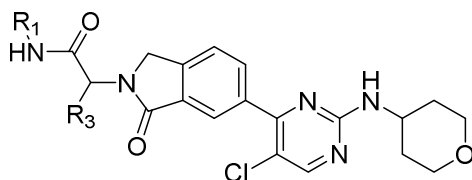
Table 1. Biochemical and cellular structure activity relationships for aminopyrimidine fragment to lead analogues.

Compound	R1	R2	R3	ERK2 IC ₅₀ / nM (n)	Prolifn IC ₅₀ / nM (n)	
					A375	Colo205
5		Me	H	76000 (1)	-	-
7		Me	H	4600 (3)	-	-
8		H	H	47000 (2)	-	-
9		F	H	57% @ 100 μM (1)	-	-
10		Cl	H	3200 (3)	-	-
11		Cl		11 (3)	1600 (1)	-
12		Cl		24 (3)	-	-
13		Cl		4.2 (3)	1200 (3)	870 (3)
14		Cl		21 (3)	34% @ 3 μM (1)	44% @ 3 μM (1)
15		Cl		4.3 (4)	660 (2)	460 (3)
16		Cl		4.0 (4)	480 (3)	670 (3)

Table 2. *In vitro* and *in vivo* pharmacokinetic parameters for selected compounds. Mice were administered a single 0.5 mg/kg dose intravenously or 5 mg/kg orally.

Compound	Permeability (Caco2, 10 ⁻⁶ cm/s)	i.v.		p.o.		
		CL (ml/min/kg)	Vdss (L/kg)	AUC (h ng/ml)	T _{1/2} (h)	F (%)
13	19	17	0.05	50	1	1
14	40	15	0.2	1800	2	32
15	17	14	0.2	530	1	8
16	22	4.2	0.1	5900	0.7	30
17	-	3.8	0.2	6900	1	32
21	15	6.0	0.08	1100	2	8
22	0.70	11	0.6	3000	3	41
24	2.2	40	1	350	3	20
25	13	23	1	2600	0.7	70
27	6.6	13	0.6	3700	0.8	59

Table 3. Biochemical and cellular structure activity relationships for benzolactam amide analogues exploring the role of the ERK1/2 back pocket.



Compound	R1	R3	ERK2 IC ₅₀ / nM (n)	Prolifn IC ₅₀ / nM (n)	
				A375	Colo205
17		H	26 (3)	45 (4)	73 (3)
18		H	4.1 (3)	91 (3)	120 (3)
19		H	68 (3)	3400 (1)	-
20		H	7.9 (3)	250 (3)	310 (3)
21		H	2.1 (3)	37 (3)	33 (3)
22		H	49% I @ 1 nM (3)	38 (3)	49 (4)
23		H	40 (3)	51% @ 10 μM (1)	-
24		H	48% I @ 1 nM (4)	7.1 (3)	7.3 (4)
25		(R)-Me	2.5 (3)	35 (3)	40 (4)
26		(S)-Me	420 (2)	-	-
27		(R)-Me	3.0 (2)	4.9 (8)	7.5 (3)

FIGURES

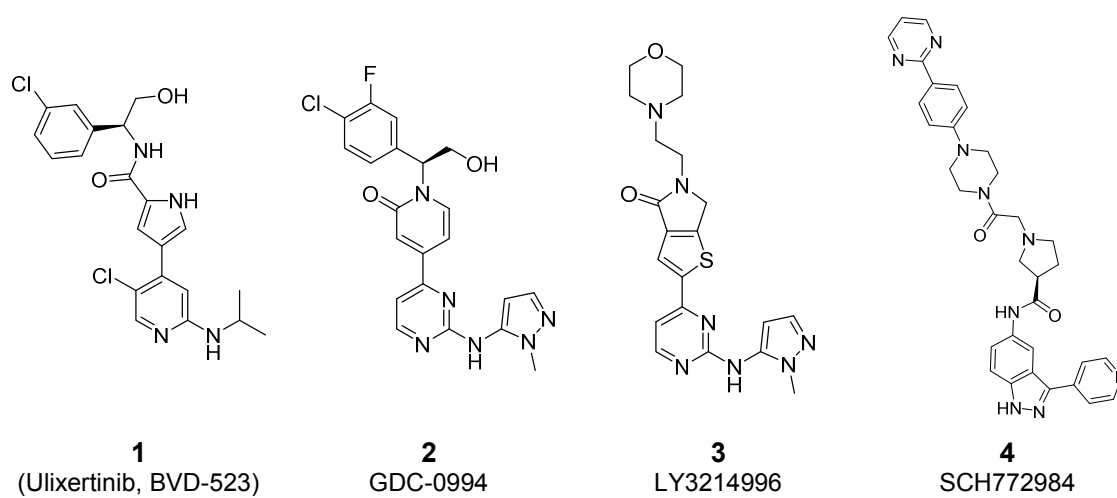
Figure 1. Chemical structures of published tool and clinical ERK1/2 inhibitors.

Figure 2. X-ray crystal structures of ERK2 obtained by soaking crystals of apo-ERK2 in the presence of each inhibitor. a) Structure of ERK2 bound to ulixertinib (**1**) with Tyr36 in “out” conformation, stacking with Tyr64 (pdb: 6gdq). b) Structure of ERK2 bound to SCH772984 (**4**) with Tyr36 in “in” conformation (pdb: 6gdm). c) Structure of ERK2 bound to aminopyrimidine fragment **5**, with Tyr36 in “out” conformation (pdb: 6g92). d) Aminoindazole fragment **6** binds both to the hinge region and the second pocket of ERK2, with Tyr36 in a third conformation pointing towards solvent (pdb: 6g8x).

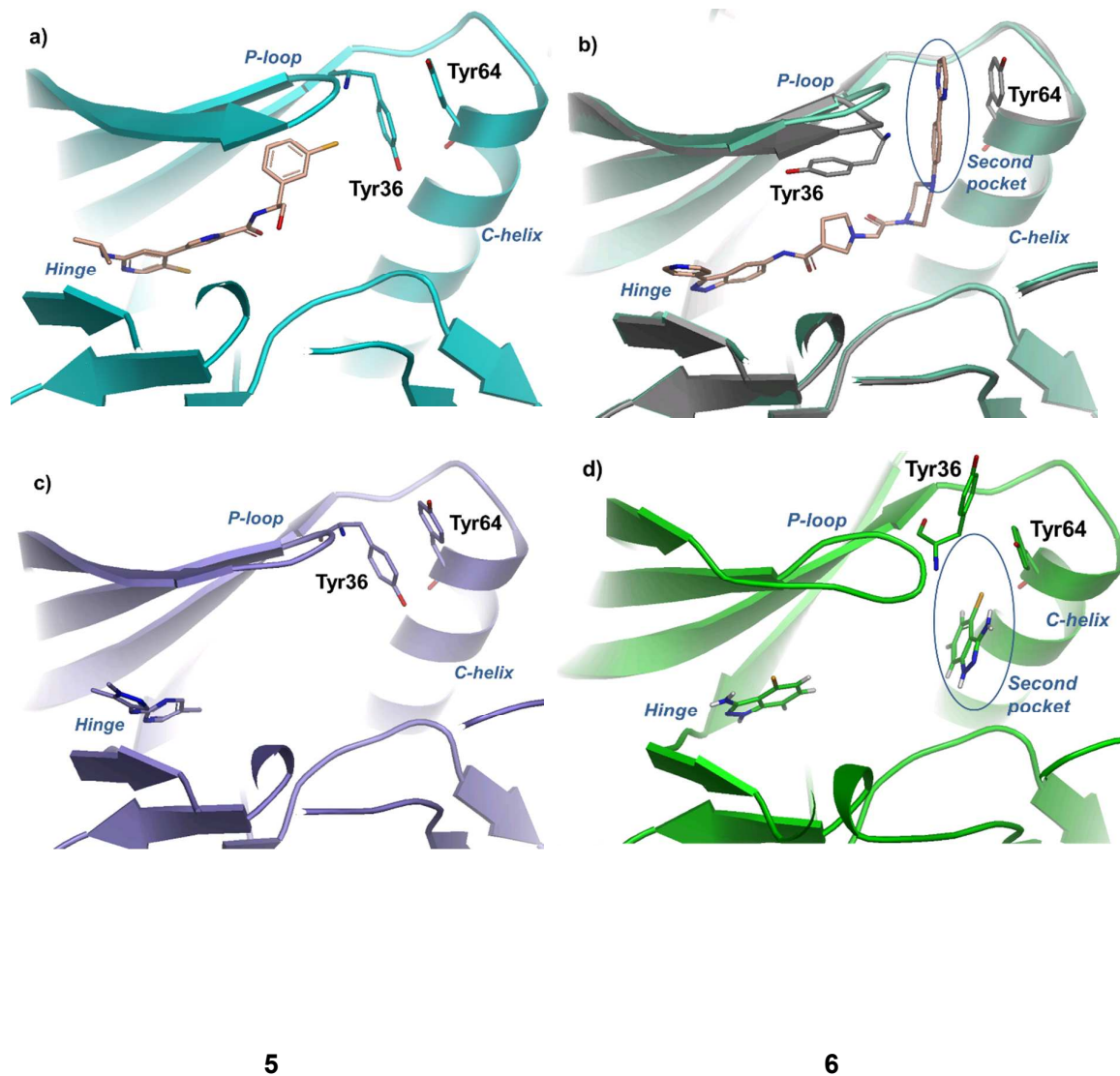


Figure 3. X-ray structures of ERK2 complexes with fragments and larger, more potent inhibitors of ERK1/2. a) ERK2 complex with Fragment **5** showing H-bonding interactions to the hinge and Lys114 (pdb: 6g92). b) Fragment **10** shows a similar binding mode, with additional halogen bond between the fragment chloro atom and gatekeeper Gln105 (pdb: 6g91). c) Overlay of ERK2 co-structures with Fragments **5** and **10** highlighting altered Lys114 conformation. d) ERK2 co-structure of benzolactam inhibitor **11**, showing additional interactions between the lactam oxygen and Gln105 (water mediated) and Lys54 (pdb: 6g93). e) Superposition of benzolactam **11** with ERK2 conformation from the complex with **4** (pdb: 6gdm), to facilitate design of compounds passing through the narrow channel into the inducible pocket (red arrow). f-g) ERK2 co-structures of t-butyl amide **15** (pdb: 6g9d) and t-butyl methyl amide **16** (pdb: 6g9h), both of which partially occupy the inducible pocket and elicit the Tyr36 “in” conformation.

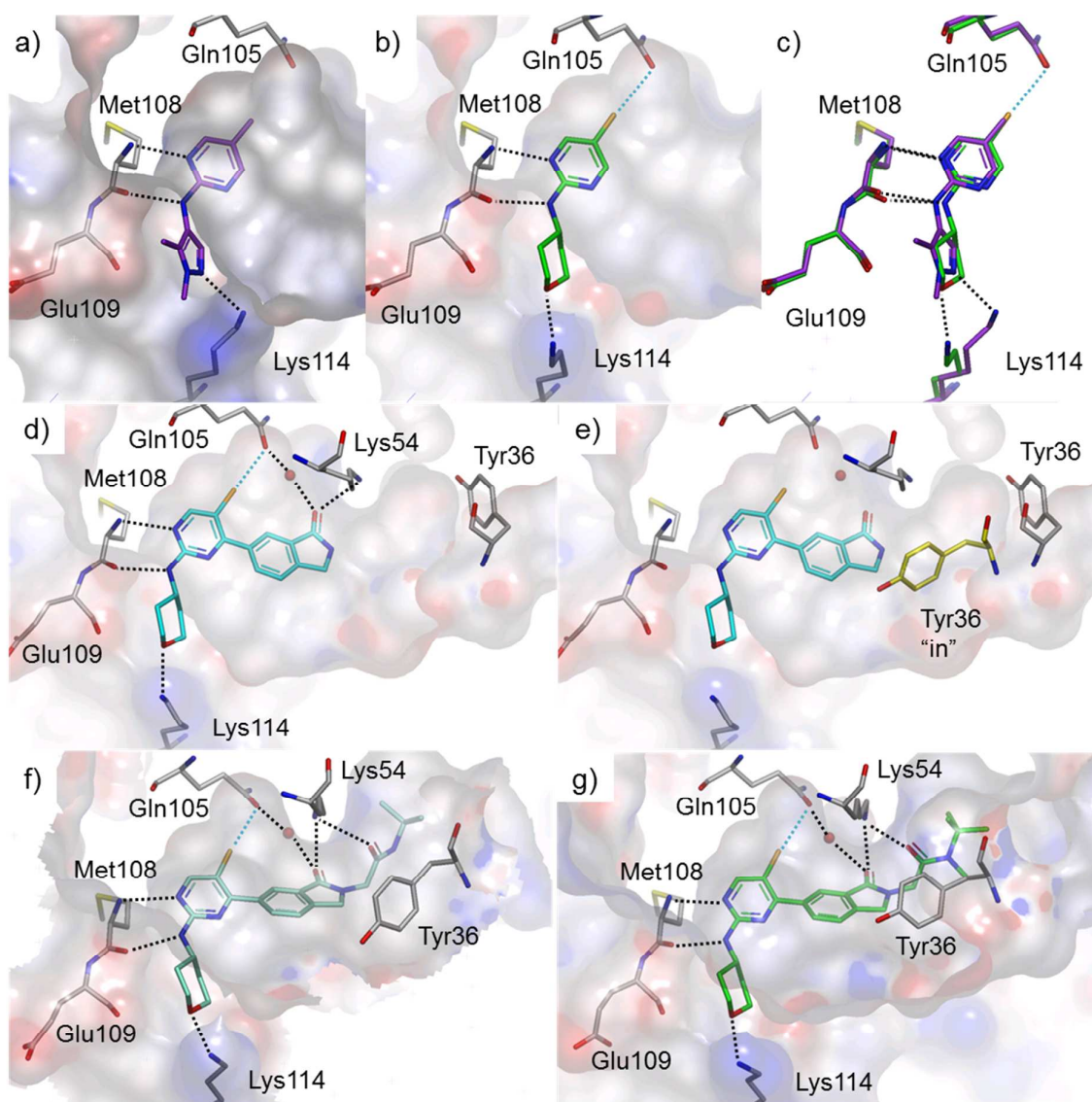


Figure 4. Pharmacological profiling of the t-butyl amide **16**. a) Effects of **16** on cellular pERK and pRSK levels. A375 cells were treated with **16** for 16 h. b) Effects of **16** on cellular pRSK levels. A375 cells were treated with **16** for 4 h and pRSK levels determined using an MSD assay. c) *In vivo* pharmacodynamic effects following a single oral 150 mg/kg dose of **16** to mice bearing Colo205 tumor xenografts. d) Anti-tumor activity of **16** dosed orally once daily at 150 mg/kg to mice bearing subcutaneous Colo205 tumor xenografts.

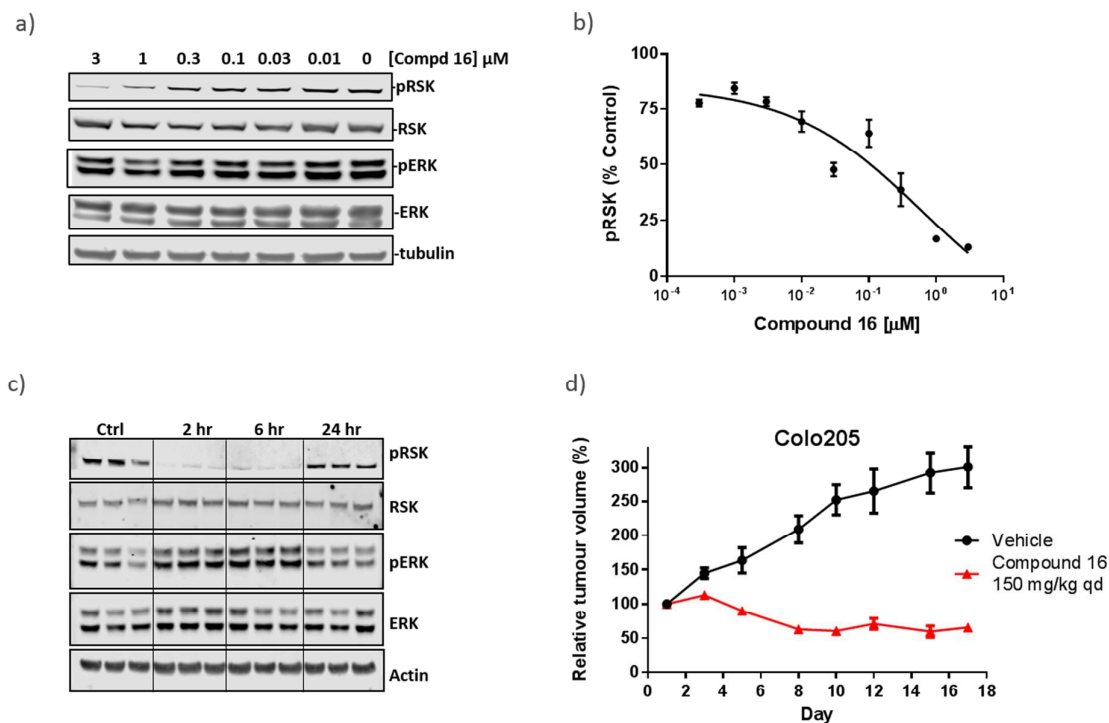


Figure 5. ERK2 X-ray co-structures of ERK1/2 inhibitors. a) Co-structure of t-butyl amide **15** showing water molecules in the solvent-accessible part of the inducible pocket adjacent to Tyr64 (pdb: 6g9d). b) Co-structure of α -methyl benzylamide **18** which occupies the inducible pocket, displacing the water molecules, and inducing a rotation in Tyr64 which engages in an edge-to-face pi-pi interaction with the inhibitor phenyl (pdb: 6g9j). c) Co-structure of α,α -dimethyl benzylamide **20** which does not occupy the inducible pocket, instead adopting a folded conformation in which the benzyl group mimics the “in” arrangement of Tyr36 (pdb: 6g9m). d) Addition of the 3-MeO group in benzyl amide **21** affords increased potency, possibly through additional stacking interactions with Arg67 (pdb: 6geo). e) The additional hydroxy group in **22** also affords additional potency, and bridges a charge-charge interaction between Arg67 and Asp167 (pdb: 6g9k). f) Structure of ERK2 complex with compound **27**, combining hydroxyl and methyl substitution of the benzyl amide with methylation of the acetamide linker (pdb: 6g9n).

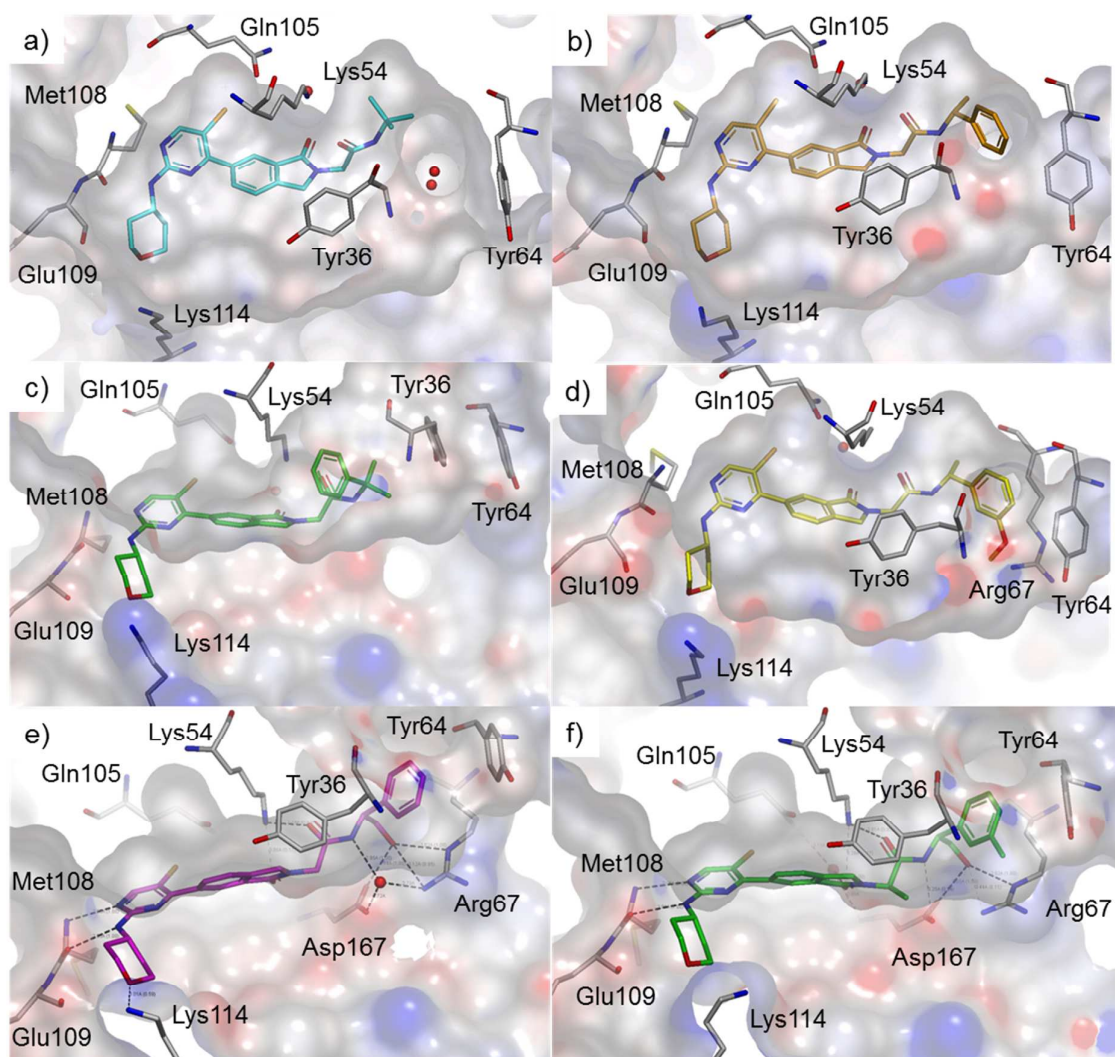
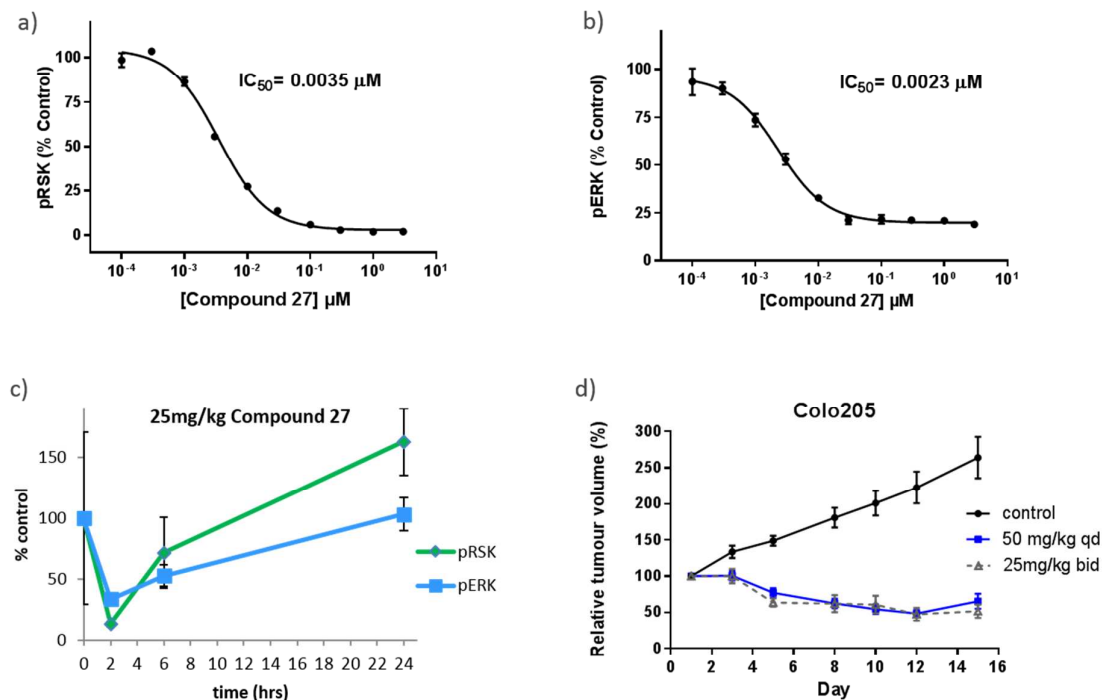
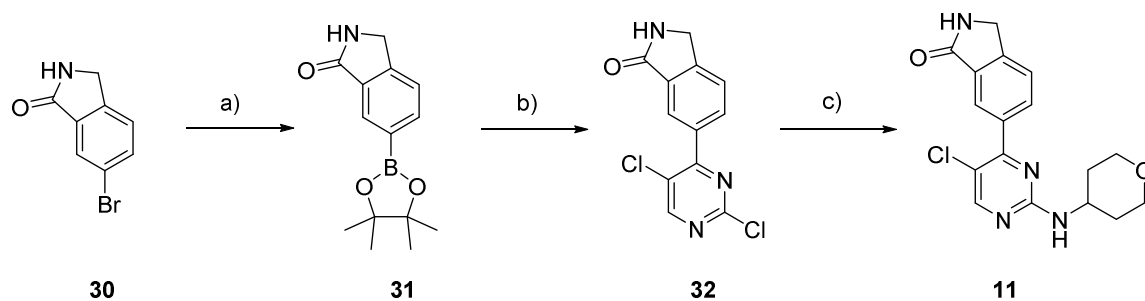


Figure 6. Pharmacological profiling of compound **27**. a) Effects of **27** on cellular pRSK levels. A375 cells were treated with **27** for 4 h and pRSK levels determined using an MSD assay. b) Effects of **27** on cellular pERK levels. A375 cells were treated with **27** for 4 h and pERK levels determined using an ELISA assay. c) *In vivo* pharmacodynamic effects following a single oral 25 mg/kg dose of **27** to mice bearing Colo205 tumor xenografts. Levels of pRSK and pERK were determined by MSD and ELISA respectively. d) Anti-tumor activity of **27** dosed orally once daily at 50 mg/kg or twice daily at 25 mg/kg to mice bearing subcutaneous Colo205 tumor xenografts.

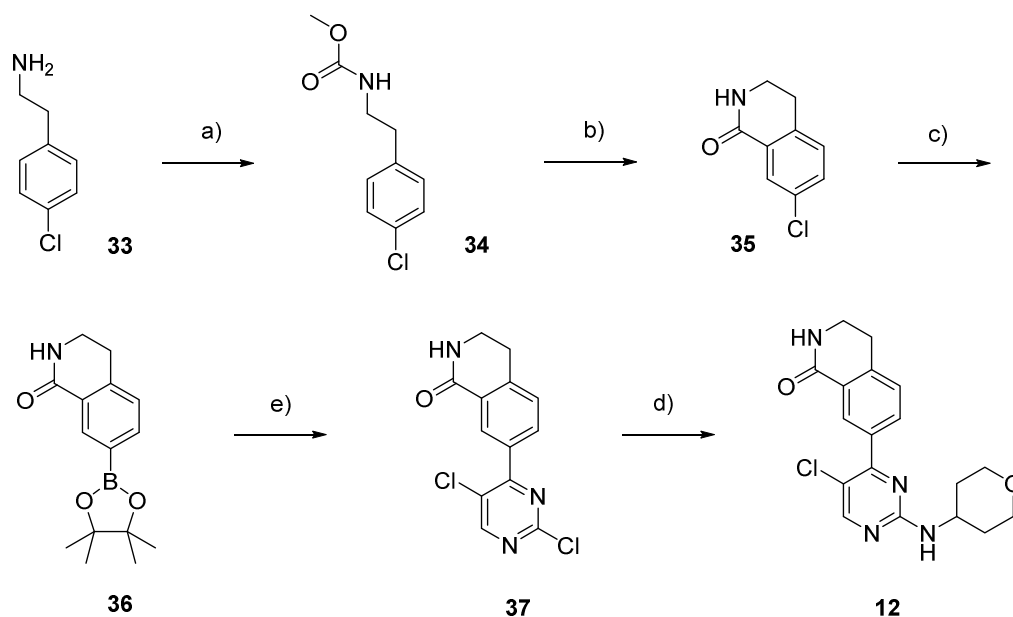


Scheme 1.



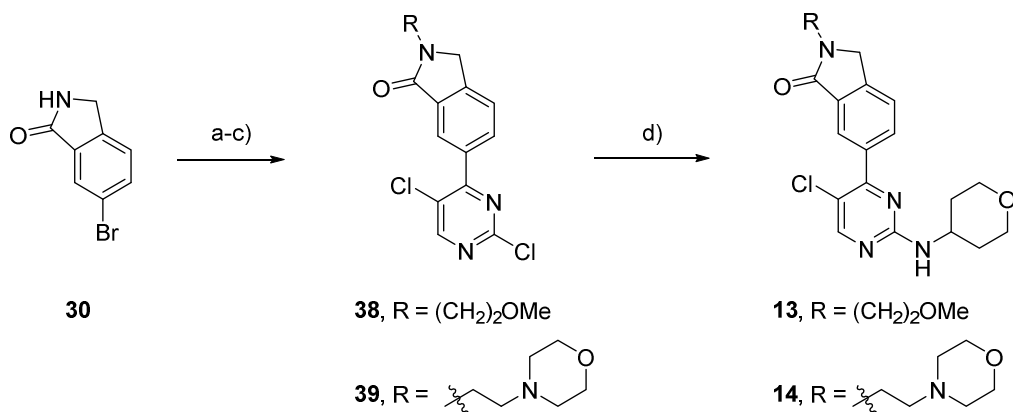
(a) Bis(pinacolato)diboron, KOAc, PdCl₂(dppf)₂, 1,4-dioxane, 100°C, 115%; (b) 2,4,5-trichloropyrimidine, K₂CO₃, Pd(PPh₃)₄, 1,4-dioxane:water (3:1), 80°C, 66%; (c) 4-Amino-oxan.HCl, DIPEA, 1,4-dioxane, 90°C, 26%.

Scheme 2.



(a) Methyl chloroformate, DIPEA, THF, RT, 2 h, 98%; (b) TfOH, 0 to 70°C, 24 h, 66%; (c) Bis(pinacolato)diboron, XPhos, KOAc, Pd₂(dba)₃, 1,4-dioxane, 80°C, 17.5 h, 106%; (d) 2,4,5-Trichloropyrimidine, K₂CO₃, Pd(PPh₃)₄, 1,4-dioxane:water (3:1), 100°C, 3 h, 71%; (e) 4-Amino-oxan.HCl, DIPEA, 1,4-dioxane, 90°C, 16 h, 28%.

Scheme 3

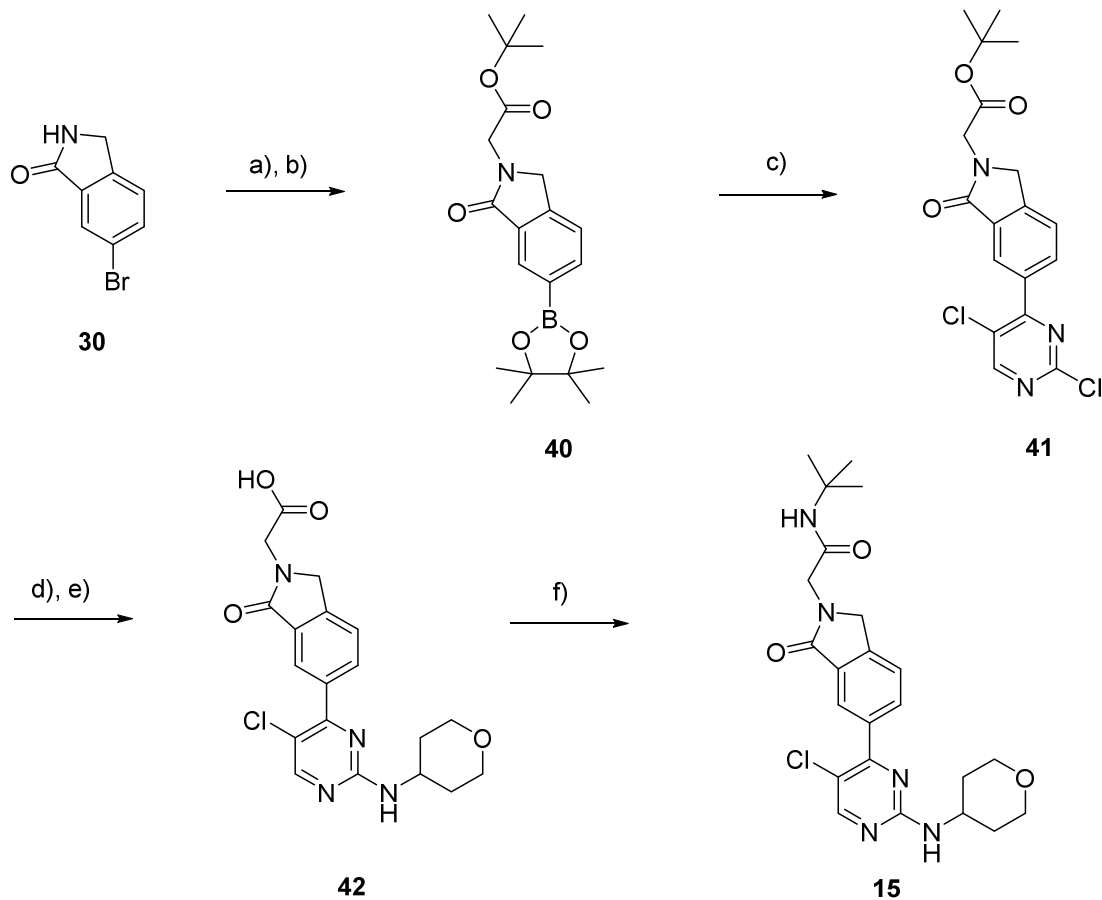


(a) NaH, RBr, DMF, 0°C; (b) bis-(pinacolato)diboron, KOAc, dioxane, PdCl₂(dppf)₂, 90°C;

(c) 2,4,5-trichloropyrimidine, SPhos-Pd G3, Na₂CO₃, dioxane/H₂O, 50°C; **38** 32%; **39** 24%.

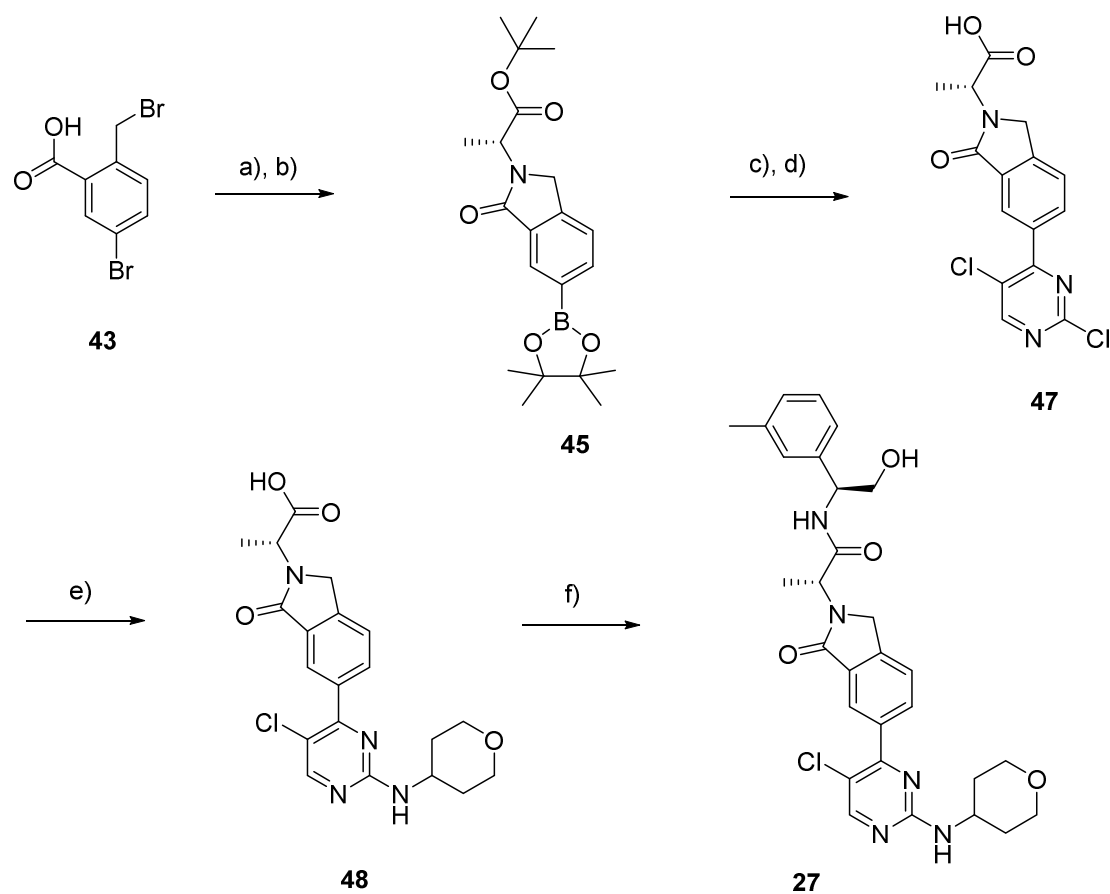
(d) Oxan-4-amine, EtN(iPr)₂, dioxane, 80°C, **13**, 53%; **14**, 30%.

Scheme 4



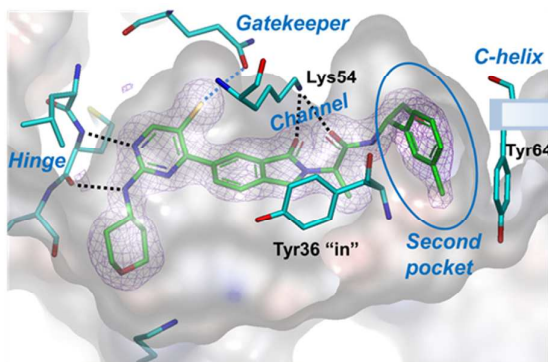
(a) NaH, RBr, DMF, 0°C, 77%; (b) bis-(pinacolato)diboron, KOAc, dioxane, PdCl₂(dppf)₂, 90°C, 75%; (c) 2,4,5-trichloropyrimidine, Pd(PPh₃)₄, K₂CO₃, dioxane/H₂O, 90°C, 62%; (d) 4-aminooxan, EtN(iPr)₂, dioxane, 80°C, 71%; e) TFA, DCM, rt, 95%; f) DIPEA, HBTU, amine, 1,4-dioxane/DMF 3:1, 70%.

Scheme 5



(a) DIPEA, (R)-tert-butyl 2-aminopropanoate hydrochloride, MeCN, 75°C, 82%; (b) bis-(pinacolato)diboron, KOAc, dioxane, XPhos Pd G3, 90°C, 94%; (c) 2,4,5-trichloropyrimidine, Pd(PPh₃)₄, Na₂CO₃, dioxane/H₂O, 90°C, 77%; (d) TFA, DCM, rt, 95%; (e) oxan-4-amine, EtN(iPr)₂, dioxane, 80°C, 78%; (f) Amine, Et₃N, TBTU, DMF, rt, 68%.

TOC GRAPHIC



2nd pocket occupancy

Suppression of both pRSK and pERK in vivo

